doi:10.1038/nature09683

Table of Contents

A) Synthetic Procedures

A1) Synthesis of known compounds. Porphyrin monomer ***l*-P1**, dimer ***l*-P2** and tetramer ***l*-P4**,[S1] hexadentate template **T6**,[S2] 1,2,3,4,5,6-hexakis[4-(4-iodophenyl)phenyl]benzene **I6**,[S3,S4] and pyrrole **1**[S5] were synthesised using published procedures.

*A2) Synthesis of figure-of-eight **c-P12·(T6)$_2$** by Vernier templating using **T6**.*

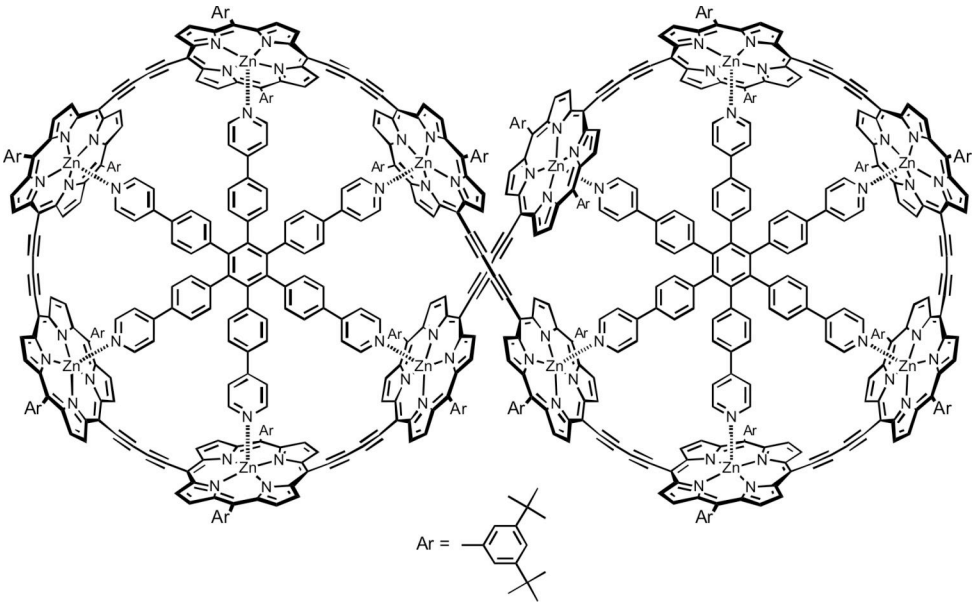

Hexadentate template **T6** (19.5 mg, 19.6 μmol) and deprotected porphyrin tetramer ***l*-P4** (61.0 mg, 19.1 μmol) were dissolved in $CHCl_3$ (88 mL) and sonicated for 1 h (bath sonicator). A catalyst solution was prepared by dissolving $Pd(PPh_3)_2Cl_2$ (17.7 mg, 25.2 μmol), copper(I) iodide (24.2 mg, 0.127 mmol) and 1,4-benzoquinone (56.1 mg, 0.52 mmol) in $CHCl_3$ (12 mL) and freshly distilled diisopropylamine (610 μL). The catalyst solution was added to the template and porphyrin tetramer mixture. The reaction mixture was stirred at room temperature for 1 h and then for 1.5 h at 50 °C under air. The mixture was passed through a plug of alumina using $CHCl_3$ as eluent, and purified by size exclusion chromatography on Biobeads SX-1 in toluene. Recrystallisation by layer addition (CH_2Cl_2 / MeOH) gave the product as a dark brown solid (29.0 mg, 39%); ^{1}H NMR (700 MHz, $CDCl_3$): δ_H 10.92 (d, 4H, J = 4.4 Hz, *β*-H), 10.16 (d, 4H, J = 3.4 Hz, *β*-H), 9.57–9.53 (m, 32H, *β*-H), 9.48 (d, 4H, J = 4.2 Hz, *β*-H), 9.30 (d, 4H, J = 3.6 Hz, *β*-H), 9.03 (d, 4H, J = 3.4 Hz, *β*-H), 8.86 (d, 4H, J = 4.4 Hz, *β*-H), 8.80–8.75 (m, 28H, *β*-H), 8.72 (d, 4H, J = 3.9 Hz, *β*-H), 8.32 (d, 4H, J = 3.4 Hz, *β*-H), 8.11 (s, 4H, Ar-*H*), 8.08 (d, 4H, J = 4.2 Hz, *β*-H), 8.06–8.02 (m, 16H, Ar-*H*), 7.89 (s, 4H, Ar-*H*), 7.83–7.74 (m, 36H, Ar-*H*), 7.37 (s, 4H, Ar-*H*), 6.98 (s, 4H, Ar-*H*), 6.40 (s, 4H, Ar-*H*), 5.53 (d, 4H, J = 9.7 Hz, -C_6H_4-), 5.49–5.42 (m, 32H, -C_6H_4-), 5.39 (d, 4H, J = 9.2 Hz, -C_6H_4-), 5.27 (d, 4H, J = 9.9 Hz, -C_6H_4-), 5.22 (d, 4H, J = 9.4 Hz, -C_6H_4-), 4.97–4.94 (m, 16H, *β*-pyridyl), 4.81 (d, 8H, J = 9.4 Hz, *β*-pyridyl), 2.22–2.19 (m, 24H, *α*-pyridyl), 1.70 (s, 36H, *t*Bu), 1.58 (m, 72H, *t*Bu), 1.55–1.54 (m, 72H, *t*Bu), 1.53–1.51 (m, 144H, *t*Bu), 1.46 (s, 36H, *t*Bu), 1.14 (s, 36H, *t*Bu), -0.64 (s, 36H, *t*Bu); *m/z* (MALDI-ToF) 11554 ($C_{768}H_{696}N_{60}Zn_{12}$, M^+ requires 11551); λ_{max} ($CHCl_3$) / nm (log ε) 497 (5.88), 766 (5.45), 803 (5.54), 882 (5.85), 840 (5.59).

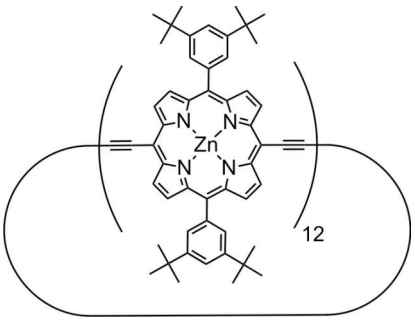

A3) Synthesis of cyclic porphyrin dodecamer ***c-P12*** *from* ***c-P12·(T6)₂.*** The figure-of-eight complex ***c*-P12·(T6)₂** (3.0 mg, 0.26 mmol) was dissolved in toluene (2 mL) and pyridine (0.2 mL) and passed over a size exclusion column (Biobeads SX-1) using a mixture of toluene and pyridine (10/1 *v/v*) as eluent. Recrystallisation by layer addition ($CHCl_3$ / MeOH) gave the product as a dark brown solid (2.4 mg, 96%); ^{1}H NMR (500 MHz, $CDCl_3$/1% d_5-pyridine): δ_H 9.84 (d, 48H, J = 4.5 Hz, β-H), 8.95 (d, 48H, J = 4.6 Hz, β-H), 8.05 (d, 48H, J = 1.5 Hz, Ar-*H*), 7.81 (t, 24H, J = 1.6 Hz, Ar-*H*), 1.56 (s, 432H, *t*Bu-CH_3); ^{13}C NMR (126 MHz, $CDCl_3$/1% d_5-pyridine): δ_C 153.0, 150.8, 150.0, 148.9, 141.8, 136.3, 133.6, 131.0, 129.4, 128.6, 125.3, 124.0, 121.3, 100.5, 84.3, 35.4, 32.1; *m/z* (MALDI-ToF) 9563 ($C_{624}H_{600}N_{48}Zn_{12}$, M^+ requires 9556); λ_{max} (toluene/1% pyridine) / nm (log ε) 472 (5.89), 488 (shoulder, 5.86), 816 (5.69).

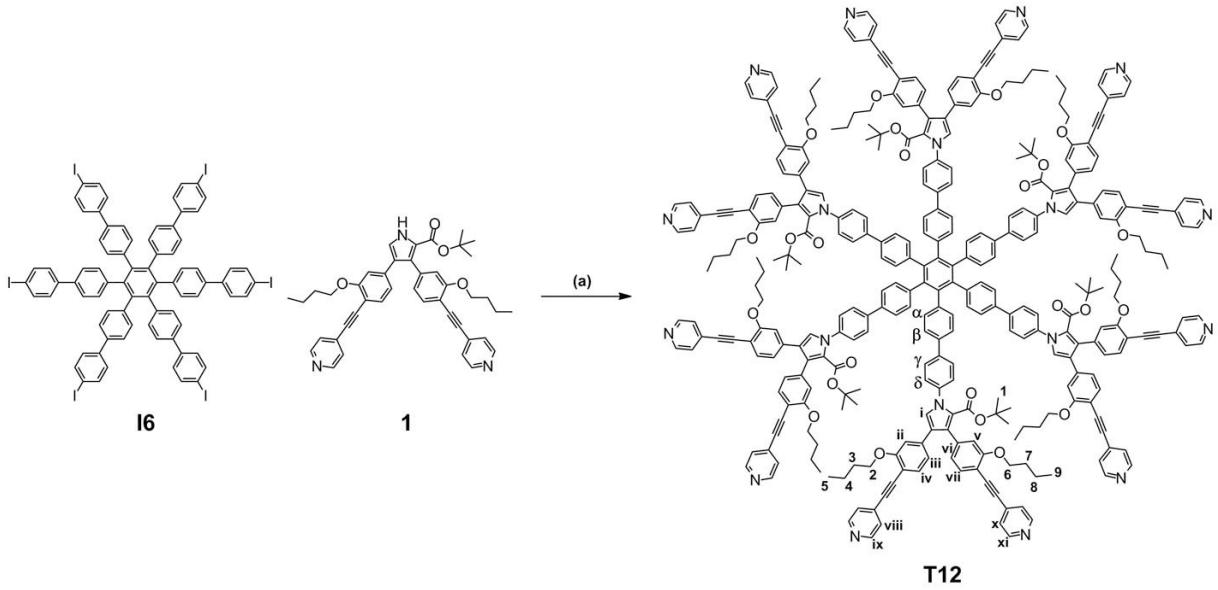

Scheme S1. Synthesis of 12-dentate template **T12**: a) *N,N'*-dimethylethylenediamine, copper(I) iodide, K_3PO_4, toluene, 110 °C, 3 d.

A4) Synthesis of 12-dentate template ***T12.*** Template **T12** was synthesised using an adapted procedure originally described by Buchwald *et al*,[S6] as shown in Scheme S1. 1,2,3,4,5,6-Hexakis[4-(4-iodophenyl)phenyl]benzene **I6** (50.0 mg, 28.6 μmol), *tert*-butyl 3,4-bis(3-butoxy-4-(pyridin-4-ylethynyl)phenyl)-1H-pyrrole-2-carboxylate **1** (381 mg, 0.57 mmol), copper(I) iodide (98.2 mg, 0.52 mmol) and potassium phosphate (474 mg, 2.23 mmol) were placed under argon. *N,N'*-Dimethylethylenediamine (222 μL, 2.06 mmol) and argon-saturated dry toluene (3.0 mL) were added, and solution degassed using the freeze-thaw method. After 3 d of stirring at 110 °C, the solvent was removed and resulting residue dissolved in dichloromethane and washed with saturated aqueous ammonium chloride. The organic layer was dried with magnesium sulfate and solvent removed. The yellow oil was passed down a short size exclusion column (Biobeads SX-1) in THF to remove excess starting material and low molecular weight side products. Fractions containing compound at R_f = 0 by silica TLC (20:1 ethyl acetate/pyridine) were collected, dissolved in dichloromethane and purified by HPLC (ACE 5 μm CN 150 × 10 mm id

column, heptane/dichloromethane/pyridine ramp, 3.5 mL/min flow rate, 313 K) to give the pure template **T12** as a pale yellow solid (4.2 mg, 4%); ^{1}H NMR (500 MHz, $CDCl_3$, 298 K): δ_H 8.61 (br s, 24H, **ix**,**xi**), 7.62 (d, 12H, J = 8.2 Hz, **β**), 7.48 (d, 6H, J = 8.0 Hz, **vii**), 7.39 (d, 12H, J = 8.2 Hz, **α**), 7.38 (br s, 24H, **viii**,**x**), 7.33 (d, 6H, J = 8.0 Hz, **iv**), 7.30 (d, 12H, J = 8.2 Hz, **γ**), 7.12 (s, 6H, **i**), 7.07 (d, 12H, J = 8.0 Hz, **δ**), 6.93 (d, 6H, J = 8.0 Hz, **vi**), 6.83 (s, 6H, **v**), 6.81 (d, 6H, J = 8.0 Hz, **iii**), 6.51 (s, 6H, **ii**), 3.94 (t, 12H, J = 6.3 Hz, **6**), 3.63 (t, 12H, J = 6.5 Hz, **2**), 1.78-1.74 (m, 12H, **7**), 1.71-1.67 (m, 12H, **3**), 1.57-1.44 (m, 24H, **8**,**4**), 1.17 (s, 9H, **1**), 0.98-0.92 (m, 36H, **5**,**9**); *m/z* (MALDI-ToF) 4974.2 ($C_{336}H_{300}N_{18}O_{24}$, M^+ requires 4974.1).

*A5) Synthesis of cyclic porphyrin dodecamer **c-P12** directed by template **T12**.* Deprotected *tert*-butyl porphyrin tetramer ***l*-P4** (7.9 mg, 2.47 μmol) and 12-dentate template **T12** (4.1 mg, 0.82 μmol) were dissolved in $CHCl_3$ (6.0 mL) and sonicated for 1 h. A solution of $Pd(PPh_3)_2Cl_2$ (1.1 mg, 1.64 μmol), copper(I) iodide (1.6 mg, 8.22 μmol) and 1,4-benzoquinone (3.6 mg, 32.9 μmol) in $CHCl_3$ (1.6 mL) and distilled diisopropylamine (80.0 μL) was added to the complex solution and stirred at room temperature for 1 h. The reaction mixture was heated to 50 °C for 1.5 h until no further change was observed by UV-vis absorption. The mixture was cooled, and the solvent removed under reduced pressure. The resulting solid was redissolved in toluene, filtered over glass wool, then passed down a size exclusion column (Biobeads SX-1, toluene) to give complex ***c*-P12·T12**. The product was analysed using UV-vis absorption (Figure S1), showing an excellent match in absorption with [12]complex obtained by titration of 12-porphyrin nanoring ***c*-P12** with template **T12**.

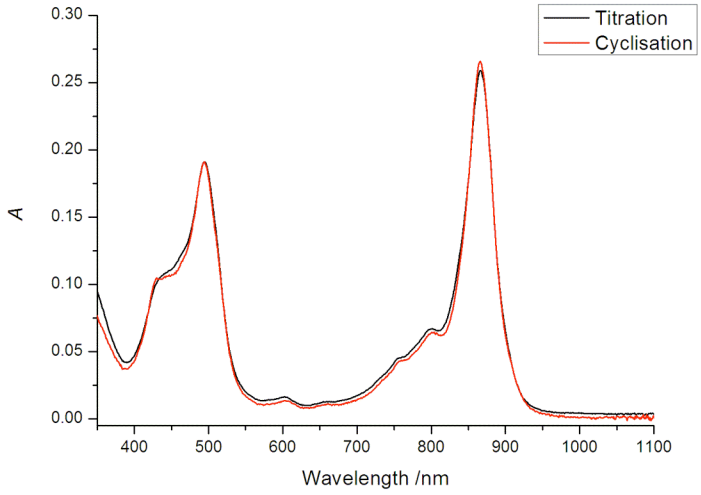

Figure S1. UV-vis absorption of [12]complex ***c*-P12·T12** obtained by titration of 12-porphyrin nanoring ***c*-P12** with 12-dentate template **T12** *(black)* and that by cyclisation of deprotected tetramer ***l*-P4** bound to 12-dentate template **(*l*-P4)$_3$·T12** *(red)*. Spectra in CH_2Cl_2, [***c*-P12·T12**] = 2.5 × 10^{-7} M^{-1}.

The complex ***c*-P12·T12** was dissolved in a 15% *v/v* pyridine/toluene mixture (2.0 mL) and sonicated for 0.5 h. The resulting solution was passed down a 30 cm size exclusion column in 15% *v/v* pyridine/toluene, and the porphyrin fraction collected. Recrystallisation in $CHCl_3$/methanol gave the 12-porphyrin nanoring ***c*-P12** (2.7 mg, 35%). ^{1}H NMR, UV-vis and GPC data for this compound exactly match those of ***c*-P12** synthesised from ***l*-P4** and **T6** by Vernier templating (see Section B5).

A6) Reference cyclisation and oligomerisation reactions.

(a) Synthesis of ***c*-P12·(T6)$_2$** from porphyrin monomer ***l*-P1** and dimer ***l*-P2**. Applying the reaction conditions specified above, Section A2, to porphyrin monomer ***l*-P1** and dimer ***l*-P2** also leads to the formation of ***c*-P12·(T6)$_2$**. However, the yields are significantly reduced (see Table S1) when compared to the reaction applying tetramer ***l*-P4**, because the main product from monomer and dimer is cyclic hexamer ***c*-P6·T6**.[S2]

Starting Material	Yield of ***c*-P12·(T6)$_2$**
Monomer ***l*-P1**	9%
Dimer ***l*-P2**	12%
Tetramer ***l*-P4**	39%

Table S1. Yields of ***c*-P12·(T6)$_2$** synthesised from ***l*-P1**, ***l*-P2** and ***l*-P4** [determined by analytical GPC, calibrated using a pure sample of ***c*-P12·(T6)$_2$**].

(b) Reaction of porphyrin oligomers in the absence of template. When applying the reaction conditions of Section A2 to porphyrins ***l*-P1**, ***l*-P2** and ***l*-P4** in the absence of any template, we observe only formation of insoluble polymeric material. This confirms the crucial role of templates in formation of cyclic species.

(c) Synthesis of cyclic dodecamer with octyloxy solubilising groups (***c*-P12^{C8}**). This compound (***c*-P12^{C8}**) was synthesised using porphyrin building blocks with 3,5-(dioctyloxy)phenyl side groups and **T6** as template. The long alkyl chains increase the solubility and appear to facilitate imaging by STM (see Section C). However, octyloxy chains increase the solubility of polymeric by-products which makes purification more complicated and leads to lower yields.

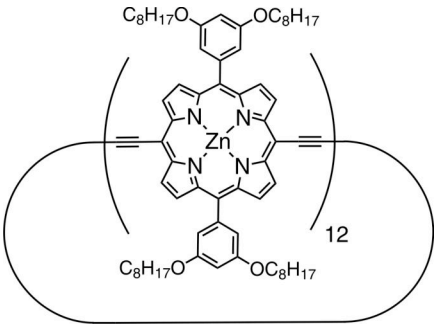

Hexadentate template **T6** (12.0 mg, 11.5 μmol) and deprotected porphyrin monomer ***l*-P1^{C8}** (50.0 mg, 46.0 μmol) were dissolved in toluene (75 mL) and sonicated for 15 min. A catalyst solution was prepared by dissolving $Pd(PPh_3)_2Cl_2$ (5.5 mg, 7.7 μmol), copper(I) iodide (7.5 mg, 38 μmol) and 1,4-benzoquinone (16.5 mg, 0.15 mmol) in toluene (5 mL) and freshly distilled diisopropylamine (0.5 mL). The catalyst solution was added to the reaction mixture. The reaction mixture was stirred at room temperature for 2 h and then refluxed for 6 h under air. The mixture was passed through a plug of alumina using toluene as eluent, and passed over a size exclusion column on Biobeads SX-1 in toluene. The first band was isolated and passed over a short size exclusion column (toluene/pyridine = 10/1) to remove the template from figure-of-eight. After drying under high vacuum for 1 h, the crude product was redissolved in CH_2Cl_2 and passed over a silica plug (eluent: CH_2Cl_2). Recrystallisation by layer addition (CH_2Cl_2 / MeOH) gave the product as a dark brown solid (2.0 mg, 2%); ^{1}H NMR (400 MHz, $CDCl_3$/1% d_5-pyridine): δ_H 9.82 (d, 48H, J = 4.6 Hz, β-H), 9.03 (d, 48H, J = 4.6 Hz, β-H), 7.38 (d, 48H, J = 2.1 Hz, Ar-*H*), 6.91 (t, 24H, J = 2.0 Hz, Ar-*H*), 4.17 (s br, 96H, -OC*H*$_2$), 1.93–1.86 (m, 96H, -OCH$_2$C*H*$_2$), 1.56–1.48 (m, 96H, -OCH$_2$CH$_2$C*H*$_2$), 1.41–1.25 (m, 384H, -C*H*$_2$), 0.84 (t, 144H, J = 6.5 Hz, -C*H*$_3$); ^{13}C NMR (126 MHz, $CDCl_3$/1% d_5-pyridine): δ_C 158.6, 153.2, 150.2, 144.6, 133.4, 131.1, 123.7, 114.8, 101.1, 100.5, 90.5, 84.2, 77.6, 68.7, 32.1, 29.8, 29.7, 29.6, 26.5, 23.0, 14.4; λ_{max} (toluene/1% pyridine) / nm (log ε) 473 (6.02), 491 (6.02), 810 (5.85).

B) Characterisation and Structure Determination

B1) Instrumentation. NMR data were collected at 700 MHz using a Bruker AVIII 700, at 500 MHz using a Bruker AVII 500 or at 400 MHz using a Bruker DPX 400. Samples were measured in $CDCl_3$ or $CDCl_3$/1% d_5-pyridine at 298 K. Chemical shifts are quoted as parts per million (ppm) relative to residual $CHCl_3$ at δ 7.27 ppm. The mixing time in the NOESY experiment for ***c*-P12·(T6)$_2$** was 200 ms. Diffusion editing of ^{1}H spectra was used to preferentially suppress solvent resonances. The bipolar-pair LED sequence (BPP-LED) was employed with a diffusion period of 50 ms and diffusion-encoding bipolar gradients of 4 ms total duration (each half-sine shaped) at 40 G/cm. A short eddy-current delay period of 5 ms was used prior to data acquisition. MALDI-ToF spectra were measured at the EPSRC National Mass Spectrometry service (Swansea) using the Applied Biosystems Voyager DE-STR. The synchrotron radiation small angle X-ray scattering (SAXS) data were collected using standard procedures on the I22 beamline at Diamond Light Source (UK) equipped with a photon counting detector. The beam was focused onto the detector placed at a distance of 1.25 m from the sample cell. The covered range of momentum transfer was $0.03 < q < 1.0$ Å^{-1} ($q = 4\pi\sin(\theta)/\lambda$ where 2θ is the scattering angle and $\lambda = 1.00$ Å is the X-ray wavelength). The data were normalised to the intensity of the incident beam; the scattering of the solvent was subtracted using an in-house program. To check for radiation damage and aggregation during the SAXS experiment, the data were collected in 10 successive 60 s frames. All SAXS measurements were performed in either toluene or toluene/1% pyridine at known concentrations (~10^{-4} M) in a solution cell with mica windows. UV-vis absorption spectra were measured on a Perkin Elmer Lambda 20 photospectrometer. Spectra were recorded at 350–1100 nm with a scan rate of 960 nm/min. Fully corrected emission spectra were measured using a custom-build system consisting of a 75 W Xenon Lamp and a nitrogen cooled InGaAs detector. Analytical GPC was carried out using PLgel 3 μm Mixed-E columns (2 × 300 mm length, 7.5 mm diameter), with a flow rate of 1 mL/min.

*B2) Figure-of-eight **c-P12·(T6)$_2$***

B2a) ^{1}H NMR analysis. As a result of the D_2 symmetry of the figure-of-eight ***c*-P12·(T6)$_2$** (three perpendicular C_2 axes through the centre, Figure S2) it is sufficient to consider only one quarter of the molecule for interpretation of the NMR spectrum. The structure drawn in Figure S2b comprises of three porphyrin units P1–P3, with P1 being the closest to the centre (marked with a red cross). The top side of the molecule, pointing away from the template is drawn in bold. The part of the template that is coordinating to these three porphyrins is also displayed.

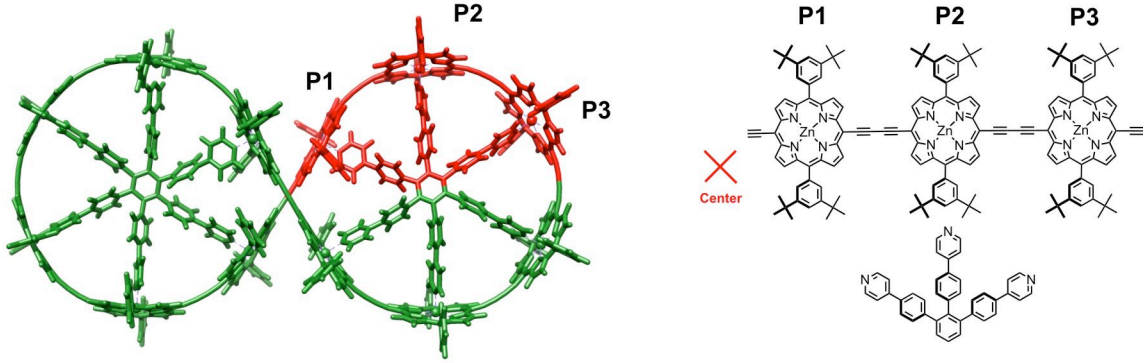

Figure S2. a) Model of figure-of-eight ***c*-P12·(T6)$_2$**; b) chemical structure of one quarter of the molecule.

Comparison with NMR data from similar compounds, such as cyclic porphyrin hexamer template complex ***c*-P6·T6**,[S2] allows for the assignment of distinct spectral regions for protons in similar environments (Figure S3): The porphyrin β-pyrrole protons are most deshielded, followed by the aryl protons. The aromatic protons of the template are more shielded due to the ring current of the porphyrin. The *t*-butyl protons appear in the alkyl region as expected.

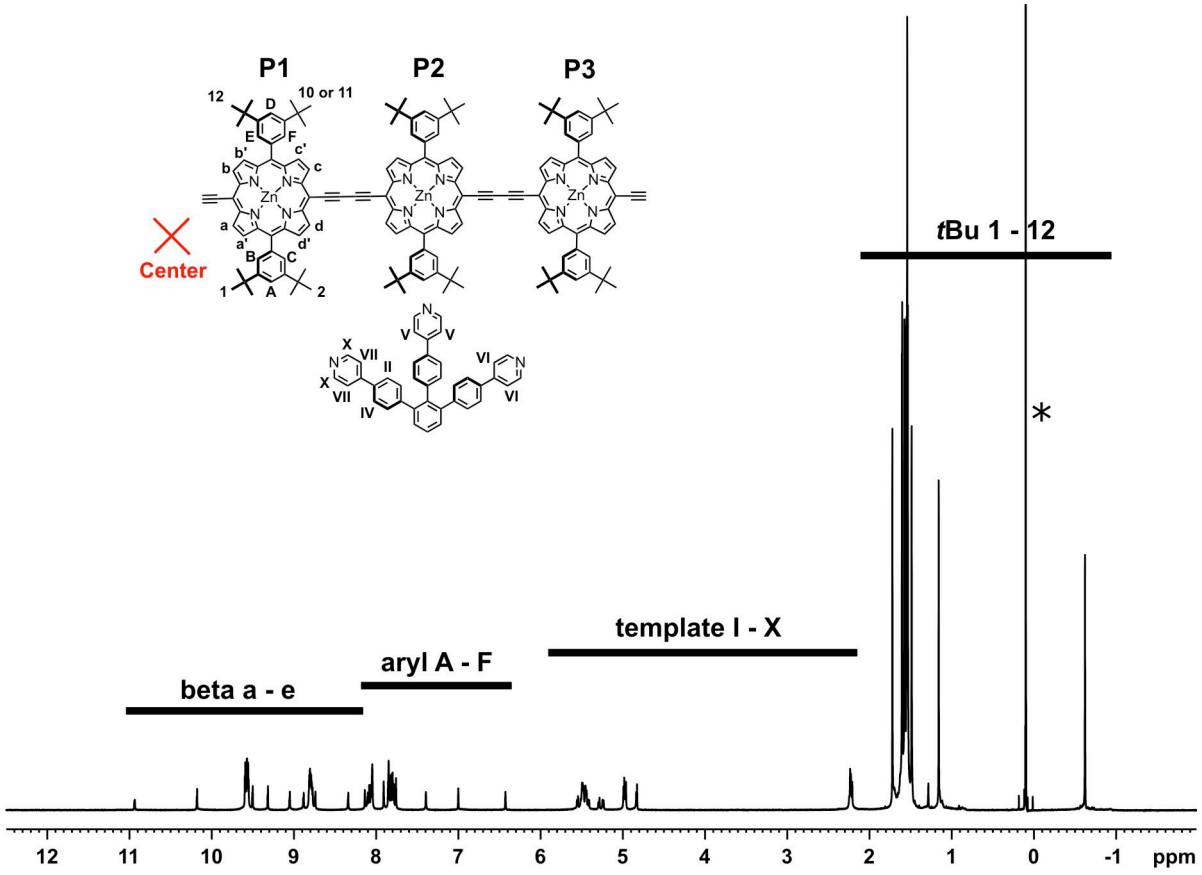

Figure S3. Diffusion-edited ^{1}H NMR spectrum of ***c*-P12·(T6)$_2$** (700 MHz, $CDCl_3$, 298 K; * indicates a silicon grease impurity).

All nine protons of each *t*Bu group are equivalent and thus result in one singlet. In each quarter of the molecule, the top and the bottom face as well as all sides are non-equivalent, which should result in 12 different signals for *t*-butyl protons. Figure S4 shows the alkyl region, which consists of the expected 12 singlets.

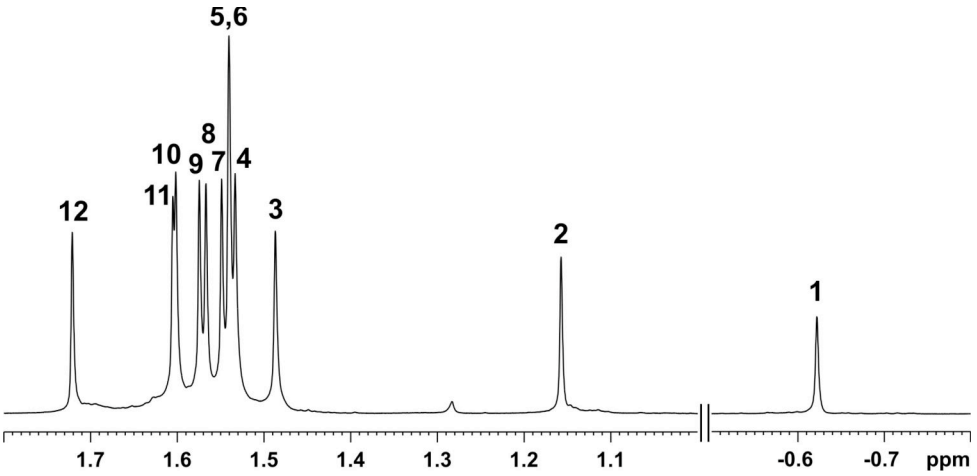

Figure S4. Alkyl region of ^{1}H NMR, showing the 12 *t*-butyl resonances of ***c*-P12·(T6)$_2$** (700 MHz, $CDCl_3$, 298 K).

The pyridyl and phenyl protons of the template are expected to be shielded by the ring current of the porphyrin macrocycles. The α-pyridyl protons (VIII–X) are closest to the porphyrin and thus, as in ***c*-P6·T6**, resonate at 2.2 ppm (see Figure S5). β-Pyridyl protons (V–VII) are less shifted and give rise to three doublets, one for each arm of the template. The inner phenyl protons (I–IV, 5.2–5.6 ppm) have the largest distance to the porphyrin and are thus least shifted. Interestingly, fully resolved phenyl peaks such as III or IV integrate to only one proton, which demonstrates that there is slow rotation of the *para*-phenylene links and that, as expected, the edges of the *para*-phenylenes are non-equivalent, whereas the pyridyl groups rotate freely.

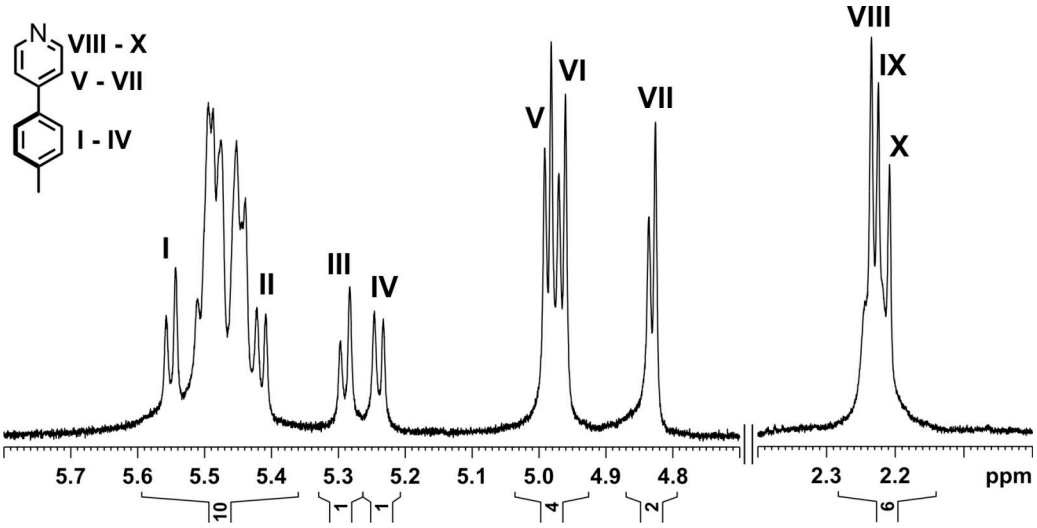

Figure S5. Region of the ^{1}H NMR spectrum showing signals of template protons (700 MHz, $CDCl_3$, 298 K).

The signals of porphyrin β-pyrrole (a–e') and aryl (A–F) protons are in the aromatic region of the spectrum, with the latter being generally more shielded. Only protons of porphyrin unit P1 can be assigned unambiguously, due to their unusual shifts. All other protons are too similar to give well separated signals, thus resulting in overlapping β-pyrrole doublets at 8.8 and 9.6 ppm as well as aryl singlets between 7.7 and 8.2 ppm.

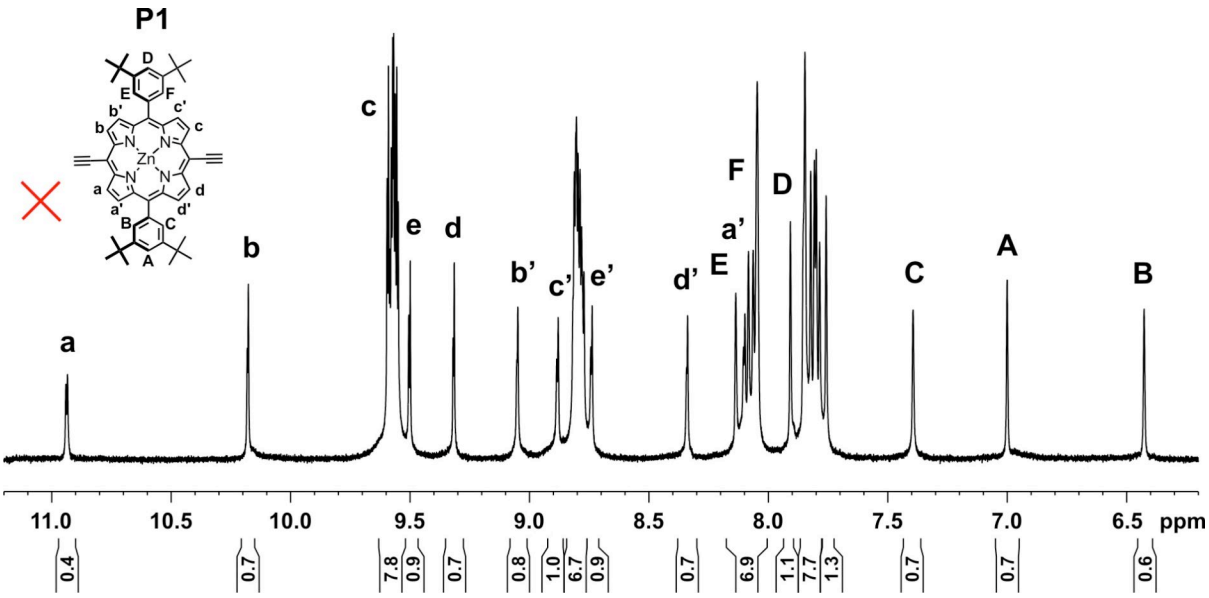

Figure S6. Aromatic region of the ^{1}H NMR spectrum (diffusion-edited, no $CHCl_3$ peak) with resonances due to porphyrin unit P1 labelled. (700 MHz, $CDCl_3$, 298 K).

Due to their unusual shift to very low frequencies and by comparison with ***c*-P6·T6**, protons VIII–X can be assigned as the α-pyridyl protons of the template. In the COSY spectrum proton VII clearly couples with X, thus the signal corresponds to the β-pyrrole protons of the same pyridyl group. Protons V, VI and VIII, IX belong to the other arms, but due to overlap, precise assignment is difficult. Proximity to the crowded centre of ***c*-P12·(T6)$_2$**, with many porphyrins in close spatial proximity should cause unusual chemical shifts and thus protons X and VII are tentatively assigned to the arm of the template coordinating to P1.

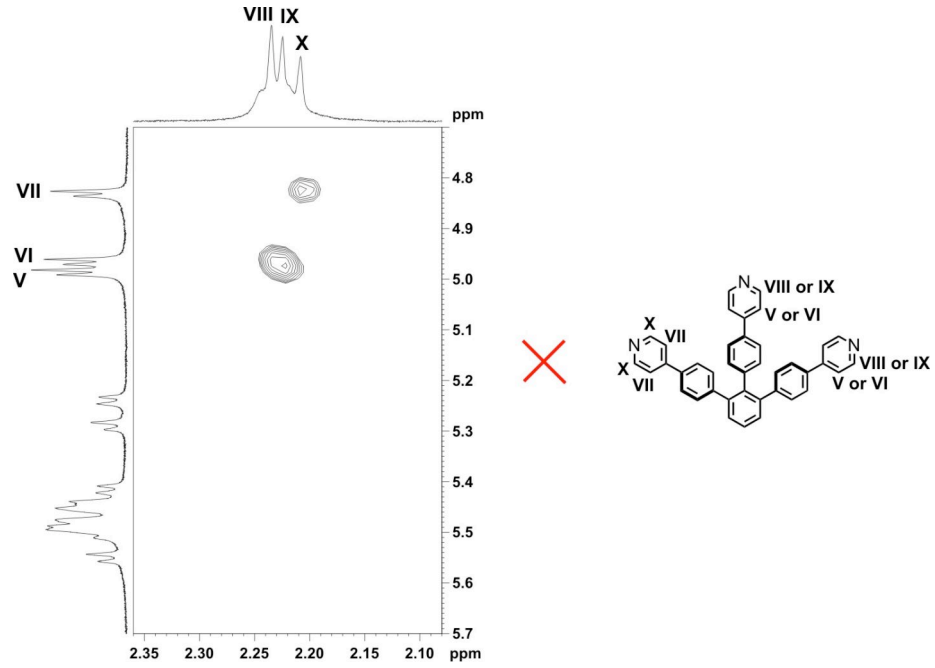

Figure S7. Part of the ^{1}H-^{1}H COSY spectrum showing coupling of pyridyl protons (700 MHz, $CDCl_3$, 298 K).

β-Pyridyl protons VII are expected to show NOEs with all eight β-pyrrole protons from porphyrin unit P1. In the NOESY seven cross peaks, plus one that overlaps with another signal, can be found and thus protons a–d can be assigned as β-pyrrole protons of P1. The widely spread chemical shifts of these eight β-pyrrole doublets give further evidence that this porphyrin is the one in closest proximity to the centre.

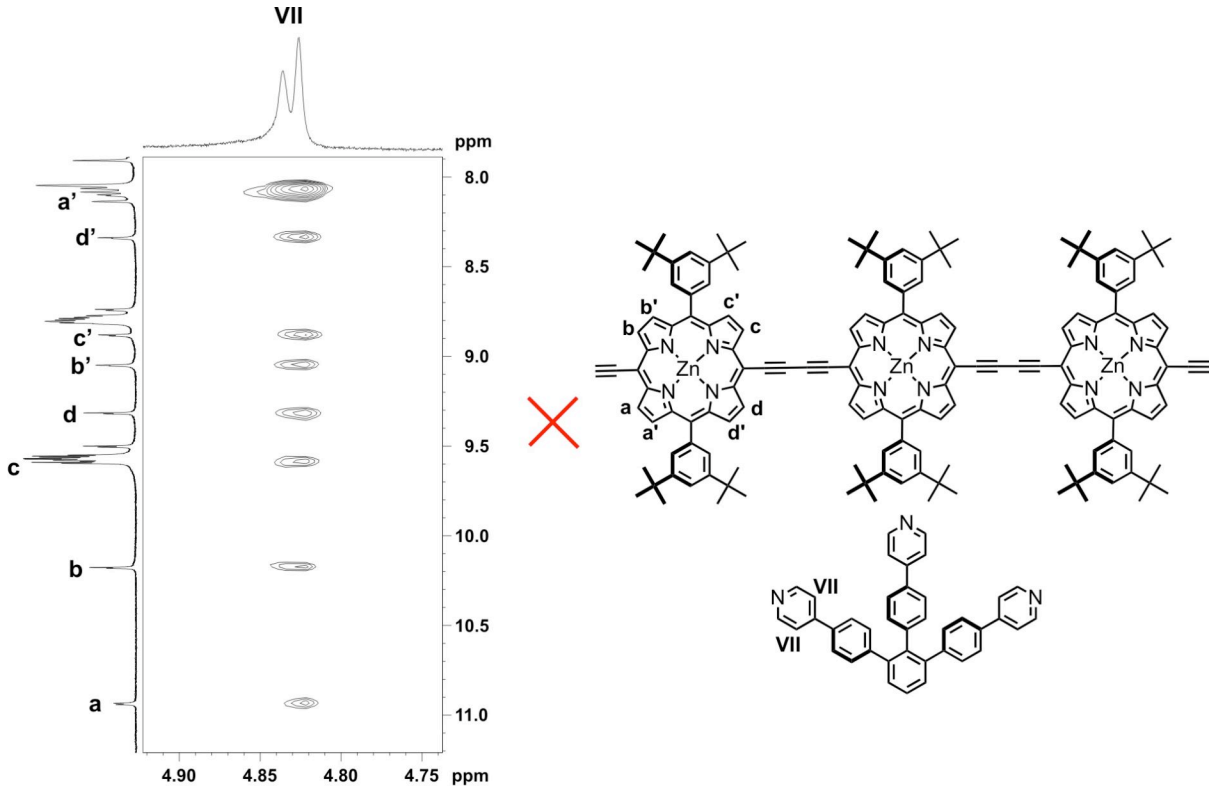

Figure S8. Part of the NOESY spectrum showing assignment of P1 β-pyrrole protons (700 MHz, $CDCl_3$, 298 K).

Having identified all P1 β-pyrrole protons, COSY allows identification of pairs such as a and a', belonging to the same pyrrole unit. For protons of P1 assignment is straightforward, whereas β-pyrrole protons of porphyrin units P2 and P3 (resonate at 9.6 and 8.8 ppm) overlap.

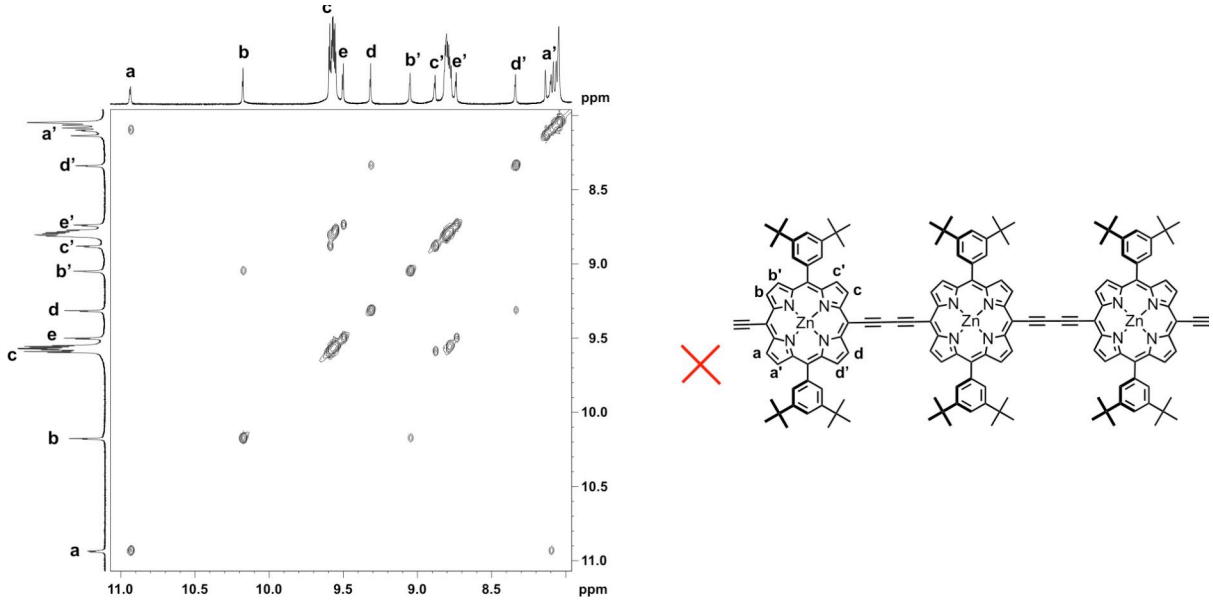

Figure S9. Part of the ^{1}H-^{1}H COSY showing coupling between porphyrin β-pyrrole protons of porphyrin unit P1 (700 MHz, $CDCl_3$, 298 K).

In the aryl region three well separated singlets A, B and C correspond to protons from the same aryl group, as confirmed by COSY.

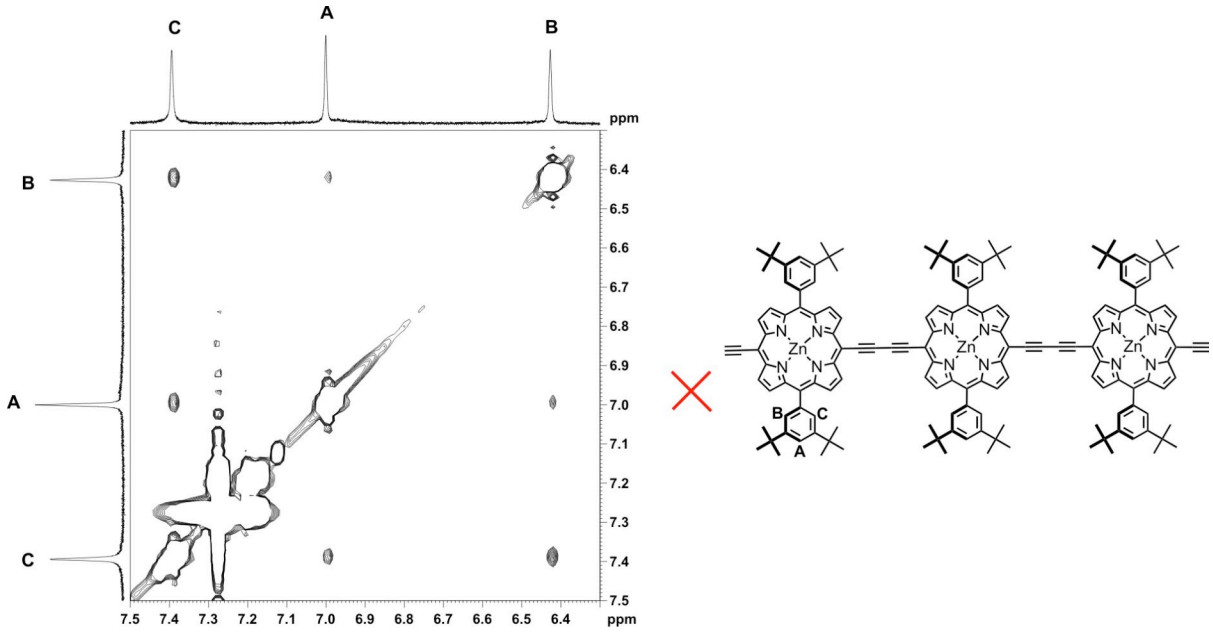

Figure S10. Selected region of the ^{1}H-^{1}H COSY showing coupling between aryl protons A, B and C of porphyrin unit P1 (700 MHz, $CDCl_3$, 298 K).

Aryl proton C shows a strong NOE with α-pyridyl proton X (Figure S11). Consequently aryl protons A–C must belong to porphyrin unit P1 with proton C pointing towards the template. Aryl protons C and B show strong NOEs with β-pyrrole protons a' and d' and weak NOE with a and d (Figure S12).

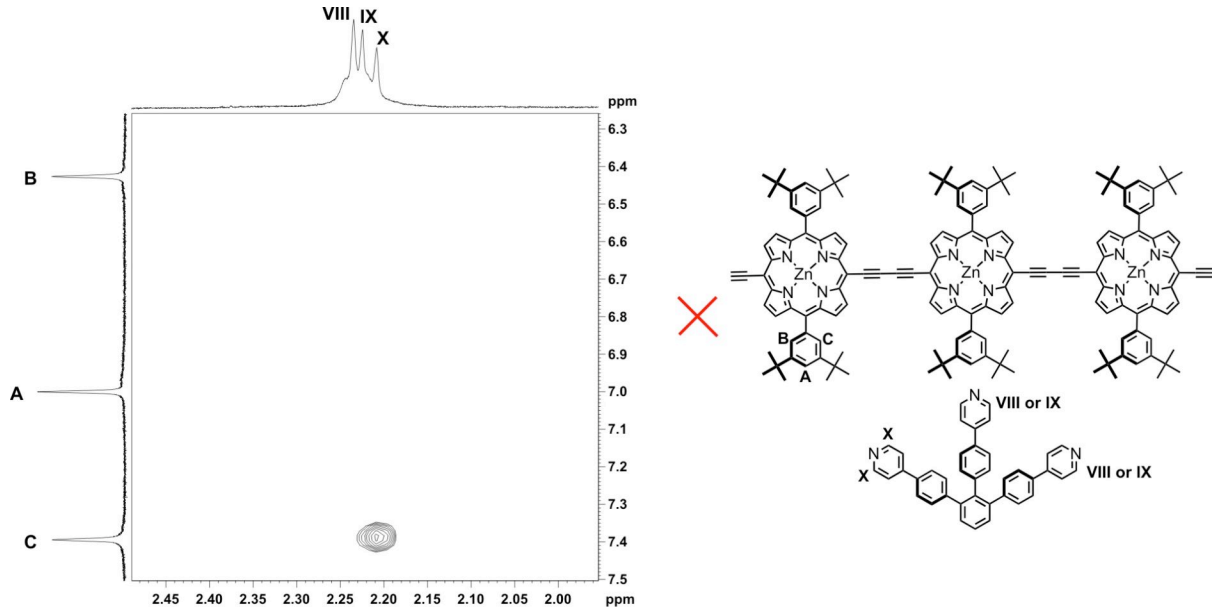

Figure S11. Part of the NOESY spectrum shows correlation between aryl proton C and template proton X (700 MHz, $CDCl_3$, 298 K).

Aryl proton A only has a weak cross peak with a' and d' which probably arises through spin diffusion processes. Thus A is in *para* position to the porphyrin and a' and d' are the β-pyrrole protons adjacent to the aryl group; a and d are adjacent to the acetylenes. The unusual shifts of A, B and C as well as β-pyrrole protons a and a' indicate that this is the side of porphyrin unit P1 pointing towards the centre of the eight. Strongly shifted protons a and a' are probably pointing towards the centre, whereas d and d' point towards porphyrin unit P2. This is confirmed by the observation of weak NOEs between d and e which belong to porphyrin unit P2 (Figure S14).

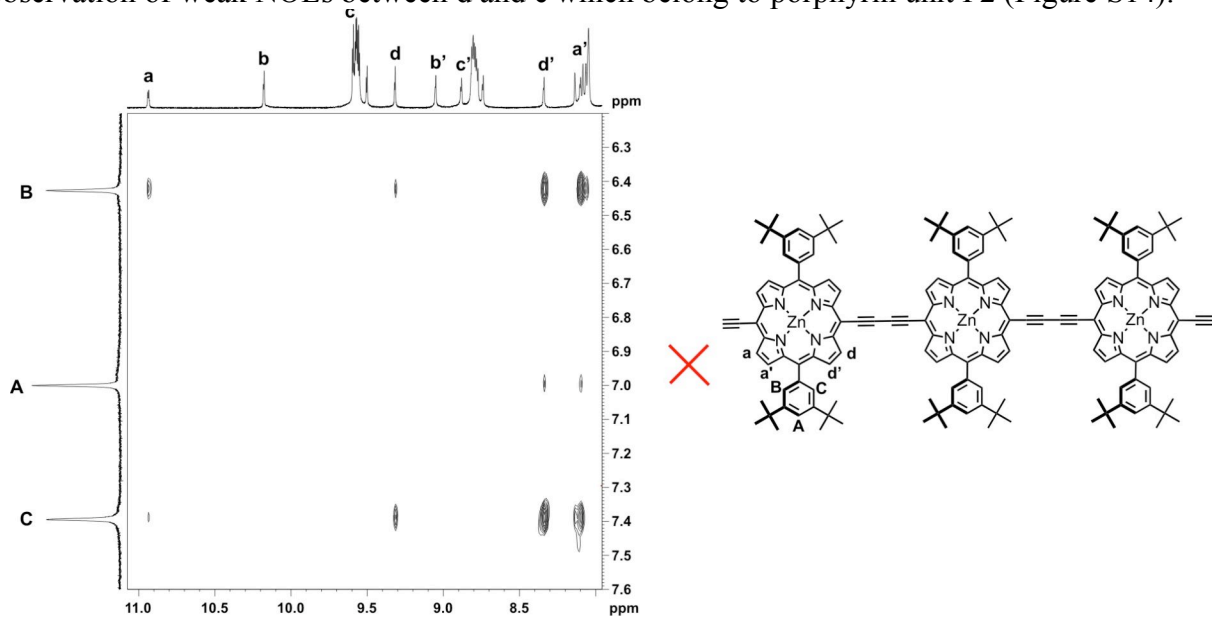

Figure S12. Part of the NOESY spectrum showing correlations between aryl and β-pyrrole protons at porphyrin unit P1 (700 MHz, $CDCl_3$, 298 K).

Interestingly, the NOE between aryl proton B (pointing away from template) and a' is stronger than with d'. At the same time the NOE between C (pointing towards template) and d' is stronger than with a' (Figures S12 and S13). These effects indicate a twist of the aryl group, with the top side leaning towards the centre of the eight. The result also indicates a certain rigidity in the centre of the molecule, that holds the aryl groups in a single conformation. Steric restrictions in the crowded centre can explain this behaviour.

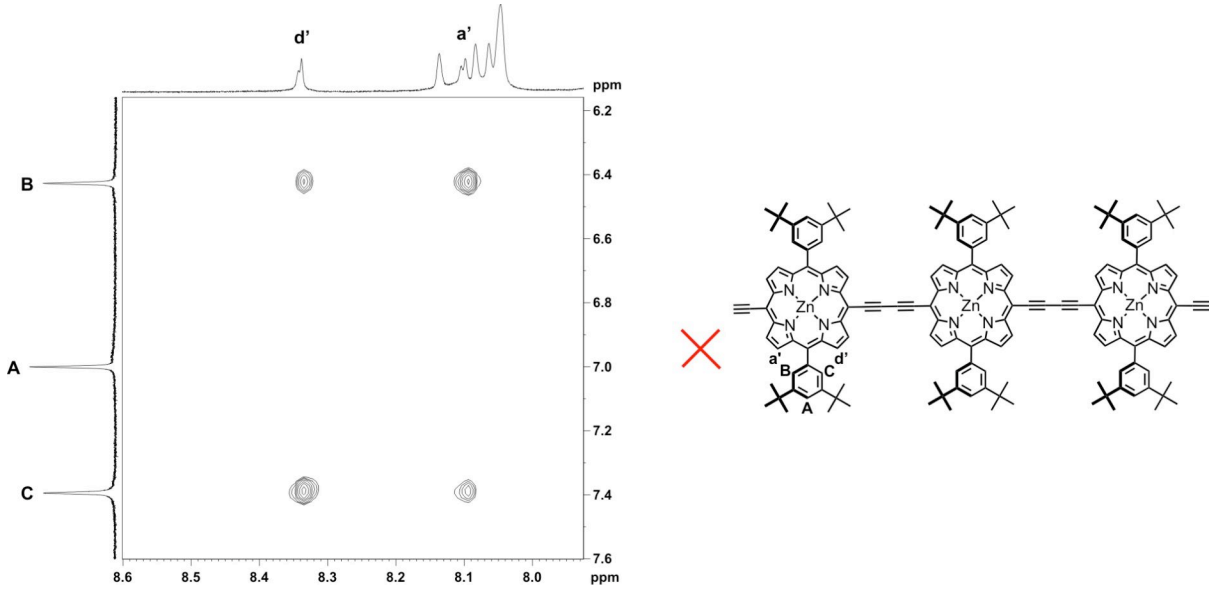

Figure S13. Part of the NOESY spectrum showing correlations between aryl and β-pyrrole protons, revealing the preferential twist of the aryl group (700 MHz, $CDCl_3$, 298 K).

As expected from COSY, β-pyrrole protons a, d and b' all display strong NOEs with their neighbouring protons a', d' and b, respectively. Additionally, each of these protons has a weaker NOE with the nearer proton on the adjacent pyrrole and consequently these can be assigned to b, c and c' respectively (Figure S14). This completes the assignment of all β-pyrrole protons at porphyrin unit P1.

There is also a weak NOE between d and e. This means that protons e and e' belong to porphyrin unit P2. However, the exact position of e and e' is unclear since c is buried under many other peaks making it impossible to exclude that c has a stronger NOE with e than has d.

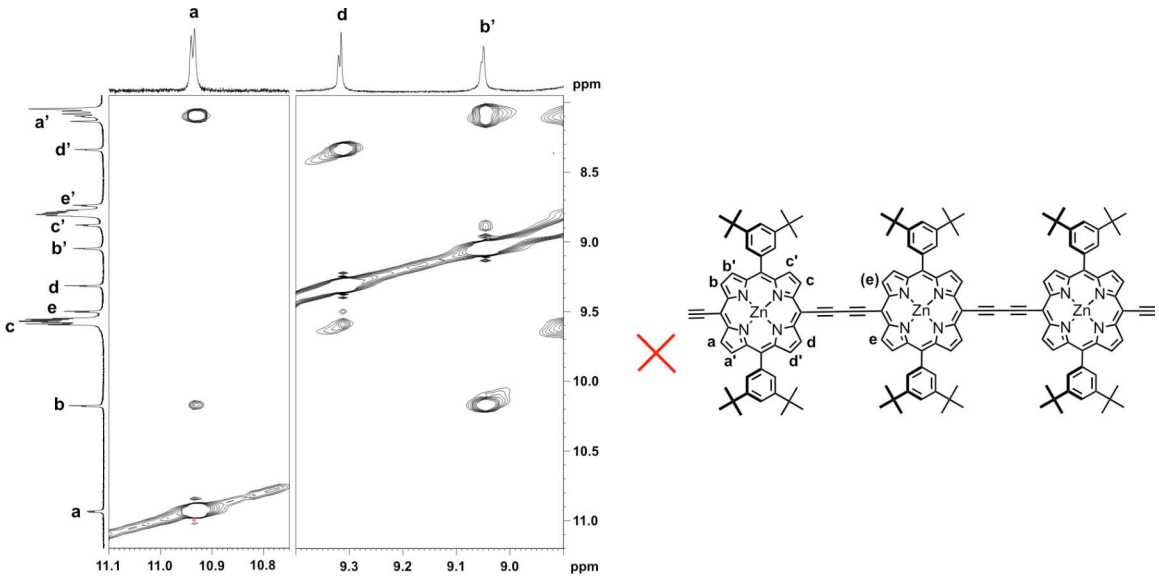

Figure S14. Part of the NOESY spectrum correlating β-pyrrole protons of different pyrroles. The third, intense crosspeak for b' arises from a NOE with the adjacent aryl proton (700 MHz, $CDCl_3$, 298 K).

Some of the *t*Bu singlets can be assigned by their NOEs with the pyridyl protons of the template. The two singlets that have stronger NOE with pyridyl protons VII belong to porphyrin unit P1 and point towards the template (2 and 10 or 11, not well enough resolved). The two signals that show weaker NOEs correspond to the protons pointing away from the template (1 and 12). These signals are likely to arise from spin diffusion. Additionally, there is a weak NOE between 2 and V. This means that V must be part of the "middle arm" of the template that coordinates to porphyrin unit P2.

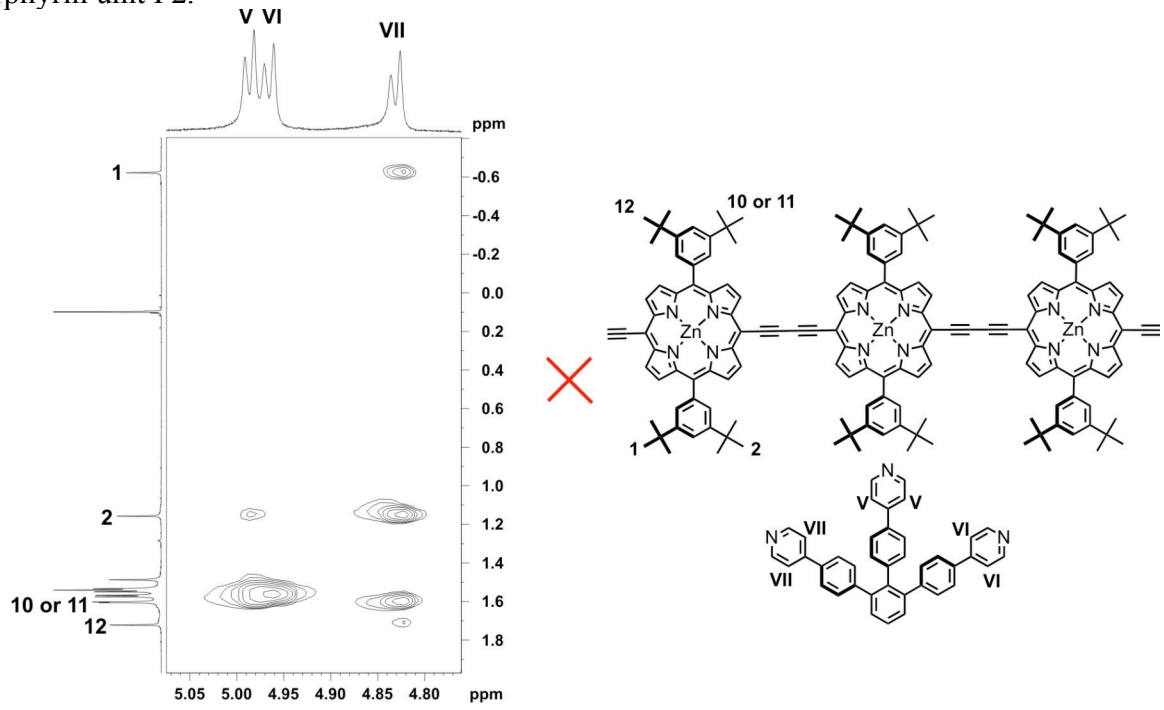

Figure S15. This region of the NOESY spectrum shows correlation of *t*Bu protons with the pyridyl protons of the template (700 MHz, $CDCl_3$, 298 K).

NOEs of *t*Bu singlets 1 and 2 with aryl signals A, B and C allows us to assign them to the aryl group that points towards the centre of ***c*-P12·(T6)$_2$**. Coupling between 1 and A as well as B confirms that this *t*Bu group points away from the template.

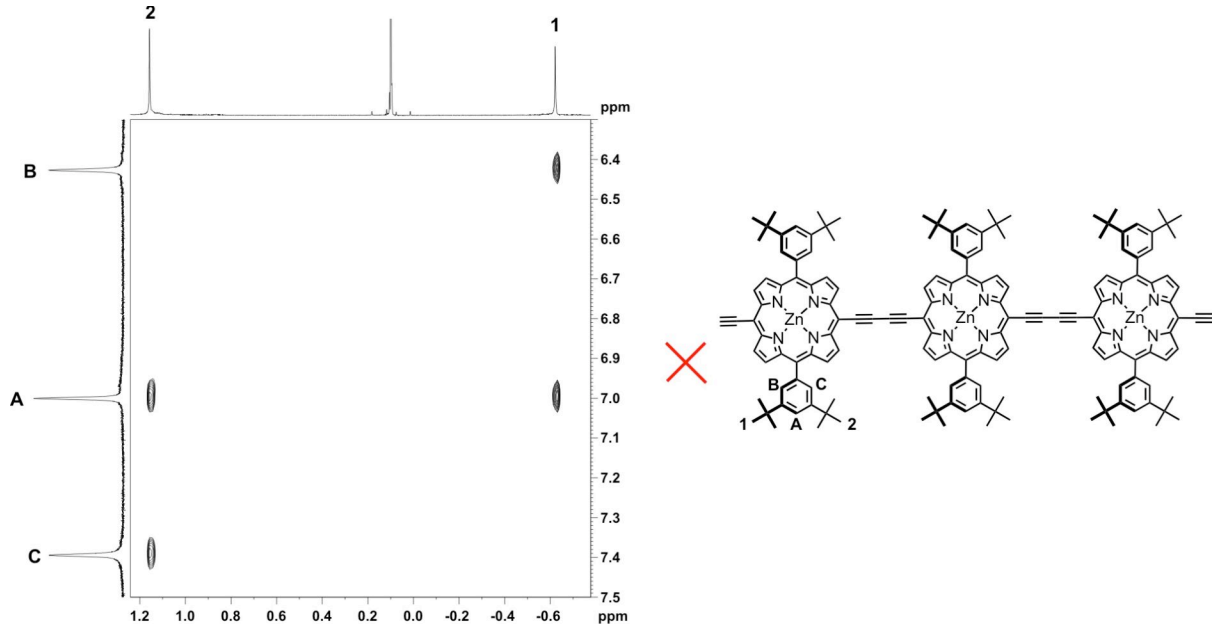

Figure S16. NOESY correlation between *t*Bu singlets and aryl protons (700 MHz, $CDCl_3$, 298 K).

The signals of the aryl group of porphyrin P1 pointing away from the centre of the eight display similar shifts to the aryl protons of porphyrin units P2 and P3. This causes partial overlap of peaks and makes assignment more difficult. NOESY shows that *t*Bu 12 (pointing outwards) is close to aryl proton E and that proton D is in *para* position to the porphyrin. Due to overlaps, aryl F cannot be directly assigned from this part of the spectrum.

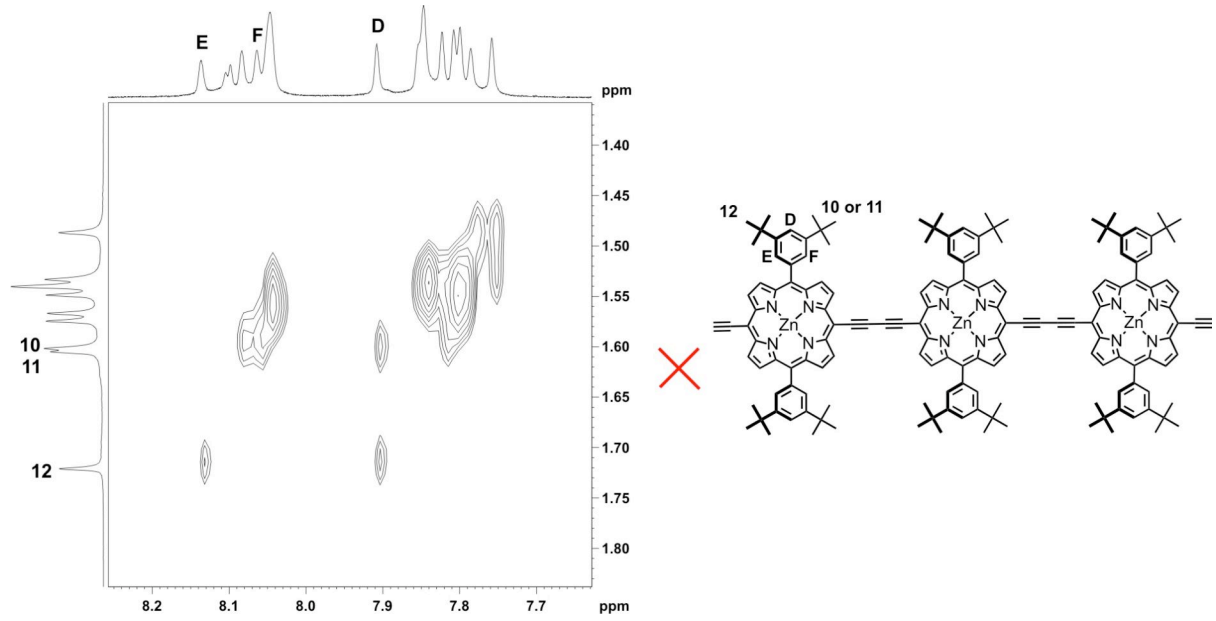

Figure S17. NOESY correlations between *t*Bu singlets and aryl protons (700 MHz, $CDCl_3$, 298 K).

Aryl proton F can be assigned unambiguously using NOEs with porphyrin β-pyrrole protons. Protons b' and c' display NOEs with aryl signals E and F but not D (pointing away from porphyrin P1). E has stronger correlation with c' than with b' and F has stronger correlation with b' than with c'. This shows that the top of the aryl group (pointing away from template) is leaning away from the centre of ***c*-P12·(T6)$_2$**. It is therefore perpendicular to the aryl group on the opposite side of P1 (Figures S18 and S13).

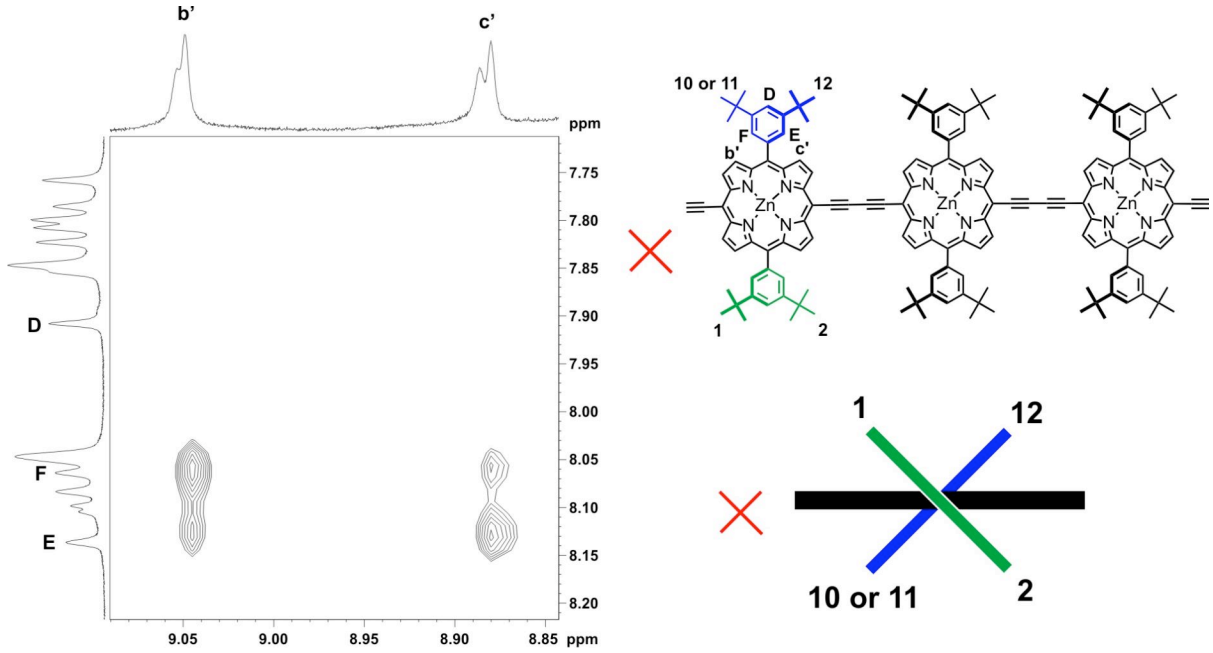

Figure S18. NOESY correlation between β-pyrrole protons and aryl protons and cartoon showing twist of aryl groups of P1 (700 MHz, $CDCl_3$, 298 K).

Further assignments of template protons can be made using both NOESY and COSY data (Figure S19). One can observe NOEs between VII and IV as well as II. These are both phenyl protons *ortho* to the phenylene-pyridyl bond, but due to hindered rotation they give different signals. In the COSY of the same region, a cross peak between IV and III shows that they belong to the same phenylene unit.

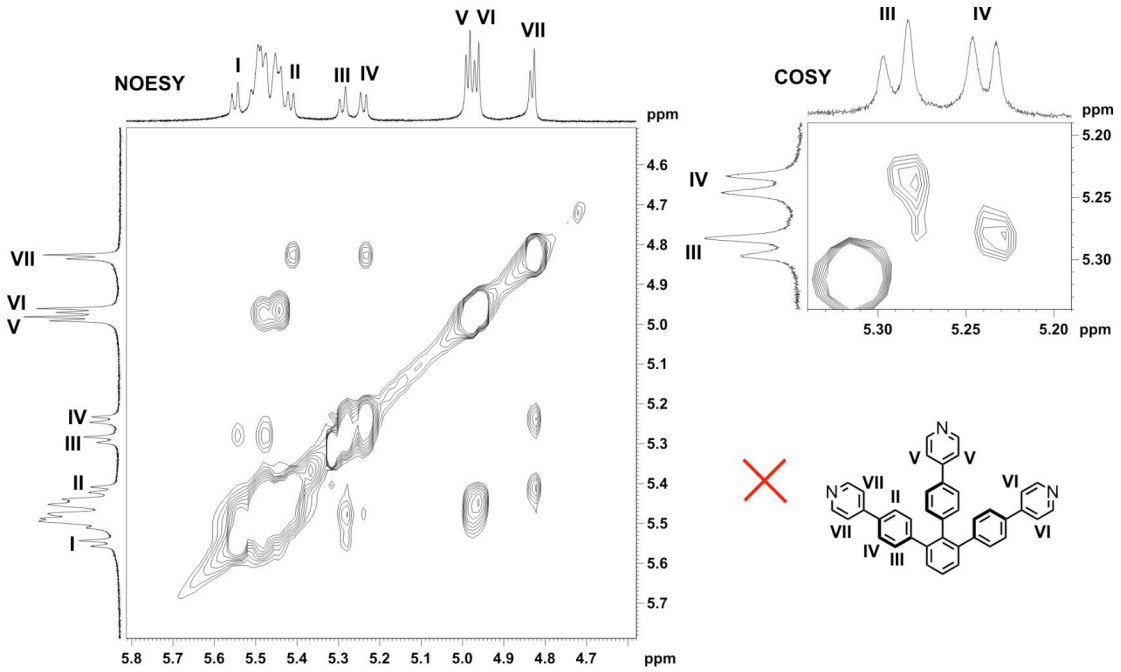

Figure S19. NOESY and COSY cross peaks between template protons (700 MHz, $CDCl_3$, 298 K). The intense diagonal crosspeak in the COSY at 5.32 ppm is due to residual CH_2Cl_2. This peak is absent in the diffusion-edited 1D projection.

NOESY data give good structural evidence for formation of the figure-of-eight using correlations between different porphyrin units in the centre of the molecule. As shown above, we find strong NOEs between β-pyrrole protons of porphyrin unit P1 and the adjacent aryl and *t*Bu protons (Figures S12 and S18). This effect is expected because of the close proximity of these protons (3–4 Å).

We can also observe strong NOEs between *t*Bu protons 1 and 2 and the β-pyrrole protons b and b', respectively, on the opposite side of P1 (Figure S20). The distance between these groups within one porphyrin is 8–9 Å, which should not result in detectable NOEs. Thus, the interaction must be between two different but symmetry related porphyrin units. This can be rationalised using the molecular model in Figure S20. In the model, the through-space distance between protons 1 and 2 of one P1 (grey, back) and β-pyrrole protons b and b' of a different P1 (black, front) are 2–3 Å. Along with symmetry arguments, these NOEs between proximate porphyrins in the centre of the figure-of-eight unambiguously confirm its structure.

If the crossing angle (between grey and black porphyrins) in the centre of the figure-of-eight was 90°, the distance of both *t*Bu groups 1 and 2 to β-pyrrole protons b and thus their NOEs would be identical. However, in the calculated structure the distance from b' to 1 is slightly smaller than to 2, which is reflected in a stronger NOE. Similar behaviour is observed between protons 1 and 2 with the more remote β-pyrrole proton c': We observe a weak NOE between 1 and c' (distance 5.9 Å) but no NOE between 2 and c' (distance 8.3 Å). These differences in the intensities of the NOEs suggest that the crossing angle must be larger than 90°, which is in agreement with the model (116°).

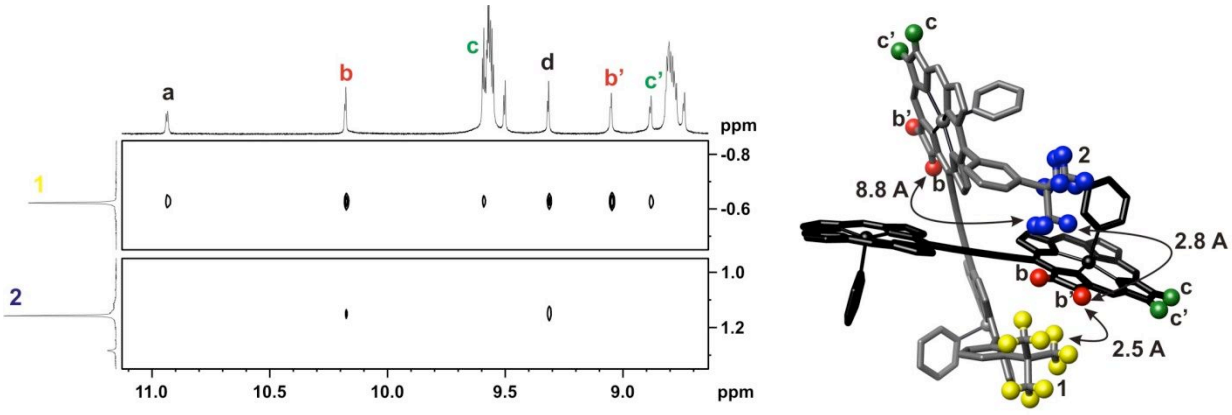

Figure S20. Interporphyrin NOEs between β-pyrrole and *t*Bu protons and model of centre of ***c*-P12·(T6)$_2$**.

B2b) MALDI mass spectrum

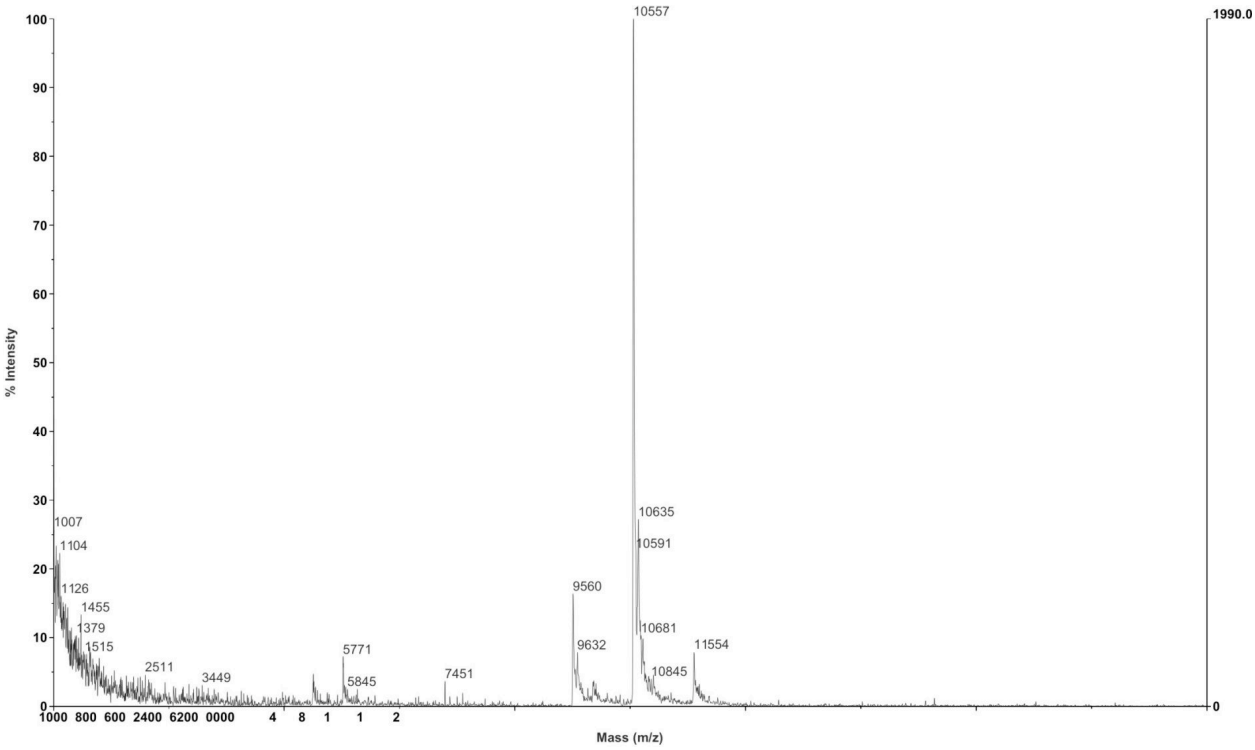

Figure S21. MALDI-ToF analysis of ***c*-P12·(T6)$_2$**. The three peaks correspond to ***c*-P12·(T6)$_2$** (*m/z* 11554, expected 11551), ***c*-P12·T6** (*m/z* 10557, expected 10554) and ***c*-P12** (*m/z* 9560, expected 9557).

B2c) SAXS analysis. The experimental scattering data were compared to a simulated scattering profile, created by the program "Crysol"[S7] using a MM+ geometry optimized molecular model. The program fits experimental parameters, such as solvent properties and solvation shell, to the experimental data. The simulated data are in very good agreement with the experimental data (Figure S22a).

The experimental scattering data can also be used to calculate the molecular weight (MW) of a molecule.[S8] The scattering intensity at zero angle $I(0)$ divided by the mass concentration (c) is directly proportional to the molecular weight of the analyte. Using a solution of ***c*-P6·T6** as a standard, we can calculate the molecular weight of the analyte molecule according to the following equation[S9]:

$$MW_X = \frac{I(0)_X}{c_X}\frac{c_{ST}}{I(0)_{ST}}MW_{ST}$$

Index x stands for the analyte and ST for the standard. The experimentally determined value for the molecular weight (11.0 kDa) is in good agreement with the calculated mass of 11.6 kDa.

At very small angles ($q \times R_g < 1.3$), the Guinier plot allows for evaluation of the monodispersity of the sample and the radius of gyration of the analyte (R_g). The scattering data in the Guinier region are very linear, confirming the monodispersity of the sample. The R_g can be obtained using the Guinier equation:

$$I(q) = I(0)\exp(\frac{-R_g^2 q^2}{3})$$

After taking the natural logarithm of this equation one can plot ln I(q) against q^2 and determine R_g from the slope of the plot. We used the program "Primus"[S8] for this purpose and obtained a slightly larger R_g value ($R_{g\ exp}$ = 20.1 Å) than for the simulated scattering profile from the modelled structure ($R_{g\ model}$ = 17.8 Å; Figure S22b).

The program "Gnom"[S10] uses indirect Fourier transformation methods to calculate the pair-distance distribution function (PDF) from raw scattering data. The PDF gives the paired-set of distances between electrons within the molecule and gives a more intuitive picture than the scattering curve. We applied the software to both the experimental and the simulated scattering data and obtained similar PDFs (Figure S22d). The distances between any two zinc atoms result in distinct peaks, because most of the electron density is located at these atoms. According to molecular mechanics calculations, the length of the molecule is 53 Å and the width 24 Å. In the PDF we observe well-resolved peaks that match these distances.

In conclusion, all four criteria–scattering data, molecular weight, radius of gyration and PDF–confirm the modelled structure of a figure-of-eight. No fit was obtained when other possible structures were modelled to the data.

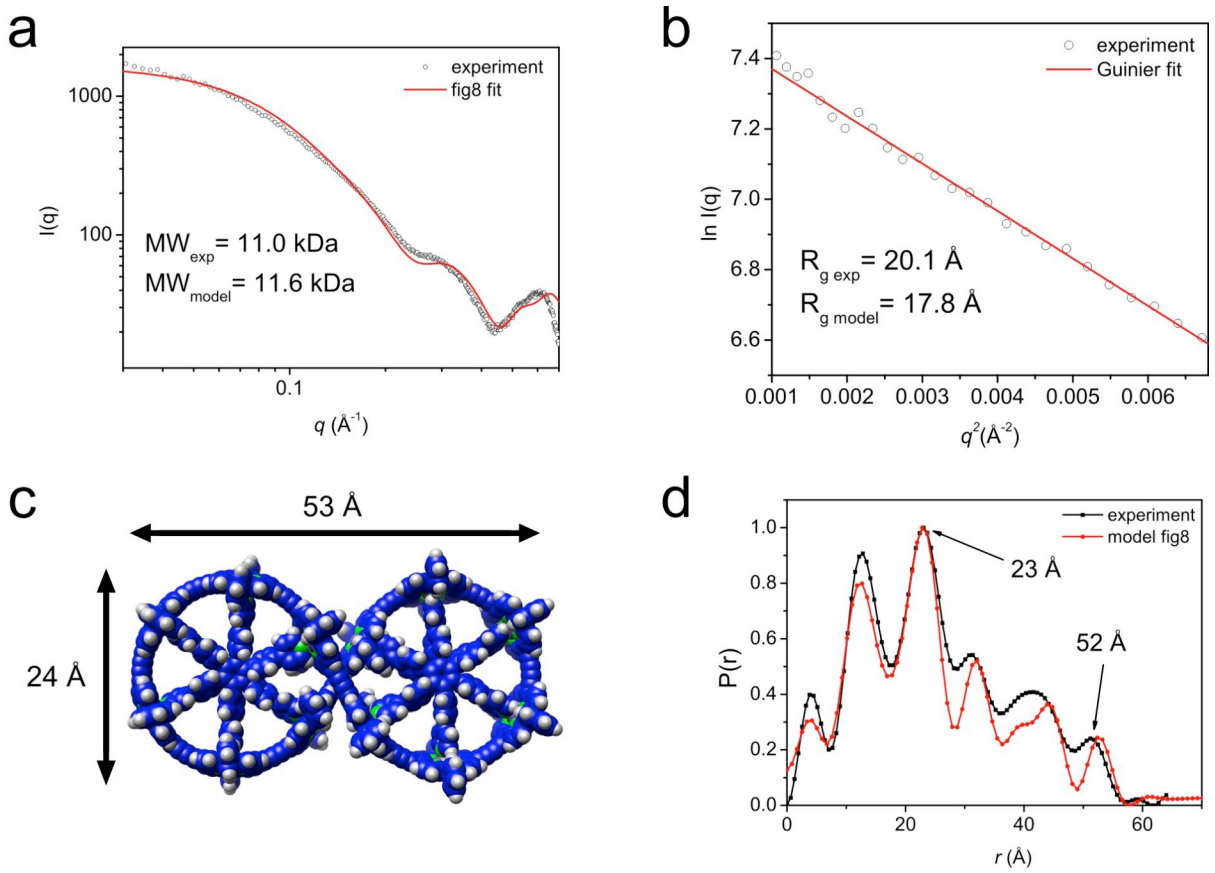

Figure S22. a) Experimental scattering curve (black circles) plotted on a double log scale with fitted data from the molecular model (red line). The experimental molecular weight was determined from the extrapolated scattering intensity at zero angle (q = 0) with ***c*-P6·T6** as standard. b) Guinier plot of the experimental scattering data (black circles) at very small angles. The fit (red line) to the Guinier equation was obtained using the software "Primus". c) Molecular model used for fitting of and comparison with experimental data. The geometry was optimised by molecular mechanics using HyperChem™'s MM+ force field. d) Experimental (black line) and model based (red) pair distribution function, obtained using the software "Gnom".

B2d) UV/vis/NIR absorption and emission spectra

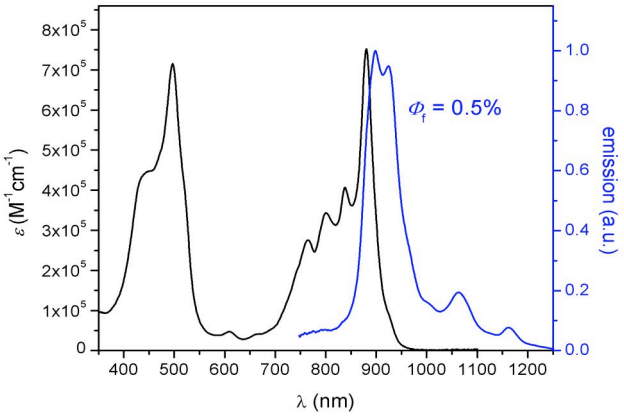

Figure S23. Optical absorption (black line) and emission spectrum (blue line, λ_{exct} = 489 nm) of ***c*-P12·(T6)$_2$** measured in toluene. Fluorescence standard for determination of the quantum yield was linear porphyrin hexamer (8.0%).[S2]

*B3) Cyclic porphyrin dodecamer **c-P12***

B3a) ^{1}H NMR analysis. The proton NMR spectrum of ***c*-P12** is very simple due to the 12-fold symmetry of the molecule. It consists of two porphyrin β-pyrrole doublets (1,2), two aryl signals (3,4) and one *t*Bu singlet. The simplicity of the spectrum is excellent evidence for formation of a single highly symmetric cyclic species.

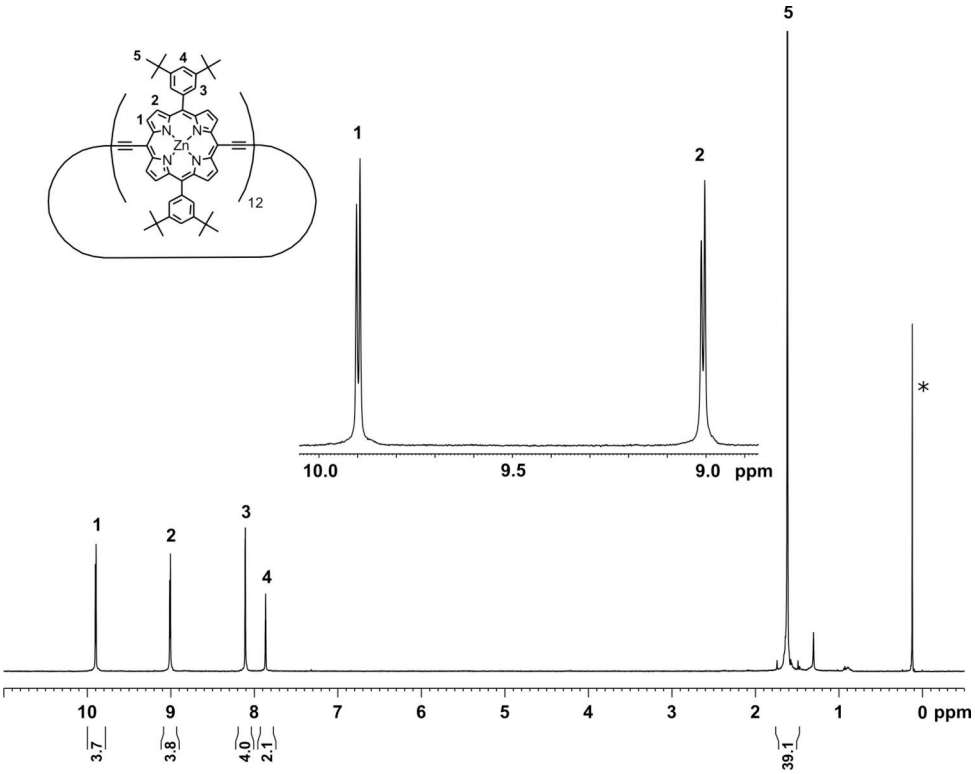

Figure S24. Diffusion-edited ^{1}H NMR spectrum of ***c*-P12** with zoom on β-pyrrole region (500 MHz, $CDCl_3$/1% d_5-pyridine, 298 K; * indicates a silicon grease impurity).

B3b) MALDI mass spectrum

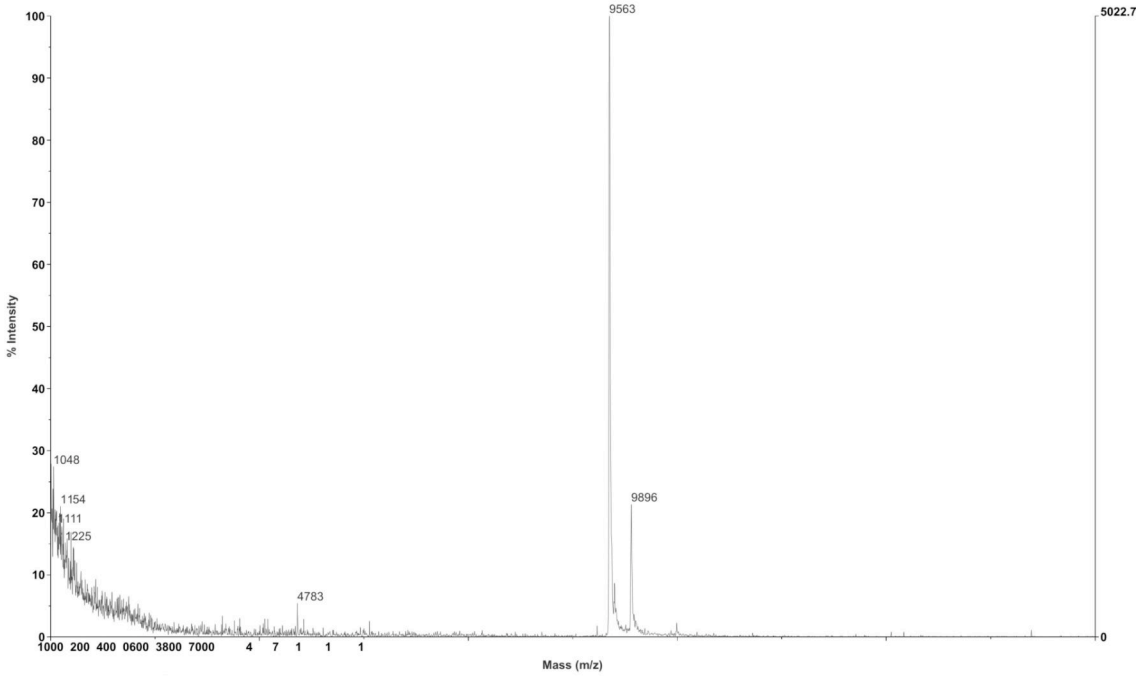

Figure S25. MALDI-ToF analysis of ***c*-P12**. The major peak corresponds to the expected mass for ***c*-P12** (*m/z* 9563, expected 9557). The origin of the peak at *m/z* 9896 is unknown.

B3c) SAXS analysis. SAXS data for ***c*-P12** were treated as described above for the figure-of-eight. However, the use of a single MM+ optimised structure did not result in acceptable fits. This is attributed to the great conformational flexibility of the molecule in solution. Molecular dynamics simulations can significantly improve the accuracy of reproducing experimental SAXS data with molecular models.[S11] Therefore we chose to use six different possible conformations of ***c*-P12** to fit the experimental data. Models were calculated by molecular mechanics using the MM+ force field and restricting the distance between two opposite porphyrins to increasingly small values (Zn–Zn distances from 47–37 Å; Figure S26c). Scattering curves were simulated for each of these structures using "Crysol", and then the average value taken to fit the experimental data. Figure S25a shows a very good overlap of the simulated scattering pattern with the experimental data. The molecular weight obtained from *I*(0) using ***c*-P6·T6** as standard (9.5 kDa) matches almost perfectly the expected value of 9.6 kDa.

The data at small angles form a straight line in the Guinier plot, confirming monodispersity of the sample. The radius of gyration is slightly overestimated by the model. The pair distribution functions matches the data obtained from the ensemble of modelled structures very well. The peaks at longer distances are significantly broadened; a result of the structural dynamics in solution.

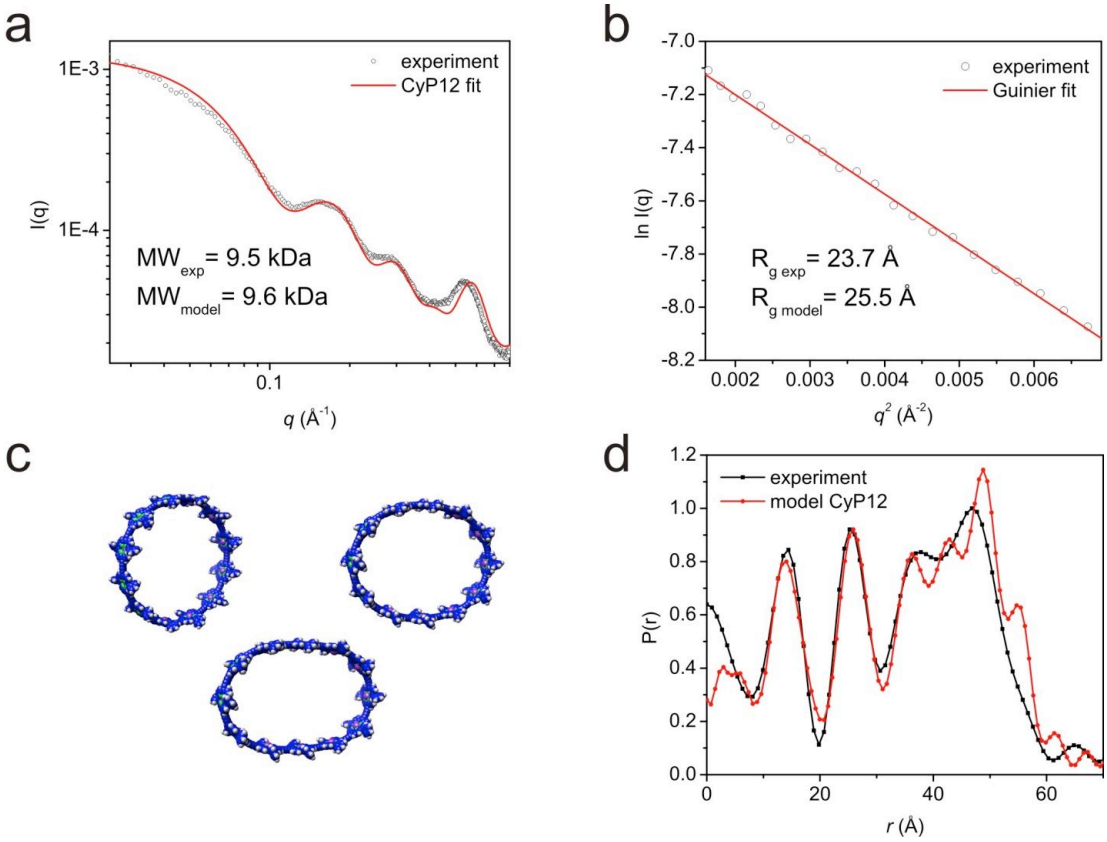

Figure S26. a) Experimental scattering curve (black circles) plotted on a double log scale with fitted data from the ensemble of molecular models (red line). The experimental molecular weight was determined from the extrapolated scattering intensity at zero angle ($q = 0$) with ***c*-P6·T6** as standard. b) Guinier plot of the experimental scattering data (black circles) at very small angles. The fit (red line) to the Guinier equation was obtained using the software "Primus". c) Three of the six molecular models used for fitting of and comparison with experimental data. The geometry was optimised by molecular mechanics using HyperChem™'s MM+ force field and restricting the distance between two opposite porphyrins. d) Experimental (black line) and model based (red) pair distribution function, obtained using the software "Gnom".

B3d) UV/vis/NIR absorption and emission spectra

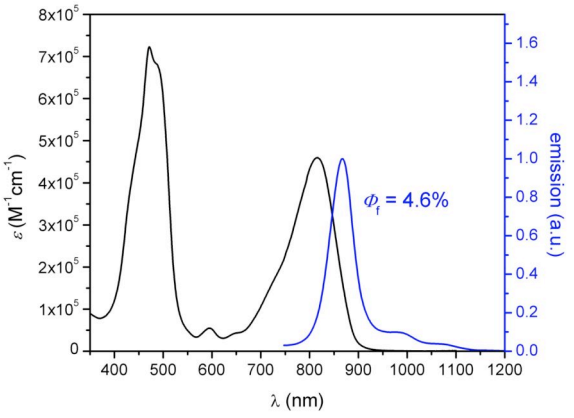

Figure S27. Optical absorption (black line) and emission spectrum (blue line, λ_{exct} = 489 nm) of ***c*-P12** measured in toluene/1% pyridine. Fluorescence standard for determination of the quantum yield was linear porphyrin hexamer (8.0%).[S2]

*B4) 12-dentate template **T12***

B4a) ^{1}H NMR analysis. The D_{6h} symmetry of the template meant that the final product should exhibit a simple spectrum resembling the summation of the two starting materials. Comparison of NMR data from the previously characterised pyrrole precursor **1**,[S5] template protons 1-9, i-xi could easily be assigned as shown in Figure S28. The chemical shifts of these resonances are very similar to those of the corresponding protons of pyrrole **1**.

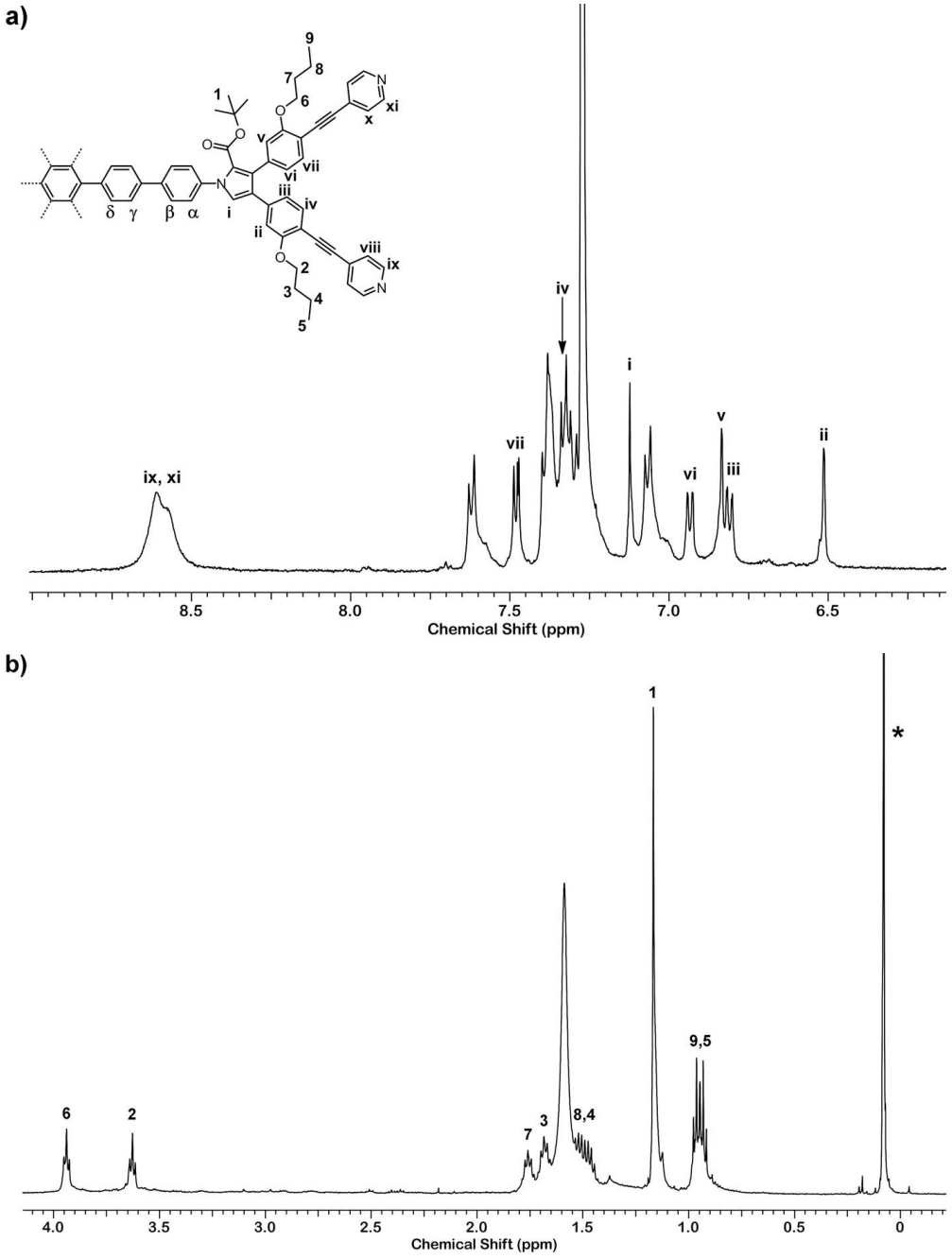

Figure S28. ^{1}H NMR spectrum (700 MHz, $CDCl_3$, 298 K) of 12-dentate template **T12**: a) Aromatic region showing pyrrole assignments; b) alkyl region of the spectrum; * indicates a silicon grease impurity.

A 1D NOESY spectrum was recorded, irradiating pyrrole proton i. As expected, NOEs with aryl protons ii and iii were observed, but it was also possible for the central hub protons α and β to be characterised (Figure S29). The crosspeak with β is not a direct NOE, but more likely a result of spin diffusion; shortening of the mixing time from 800 ms to 500 ms resulted in a dramatic decrease in the intensity of this peak.

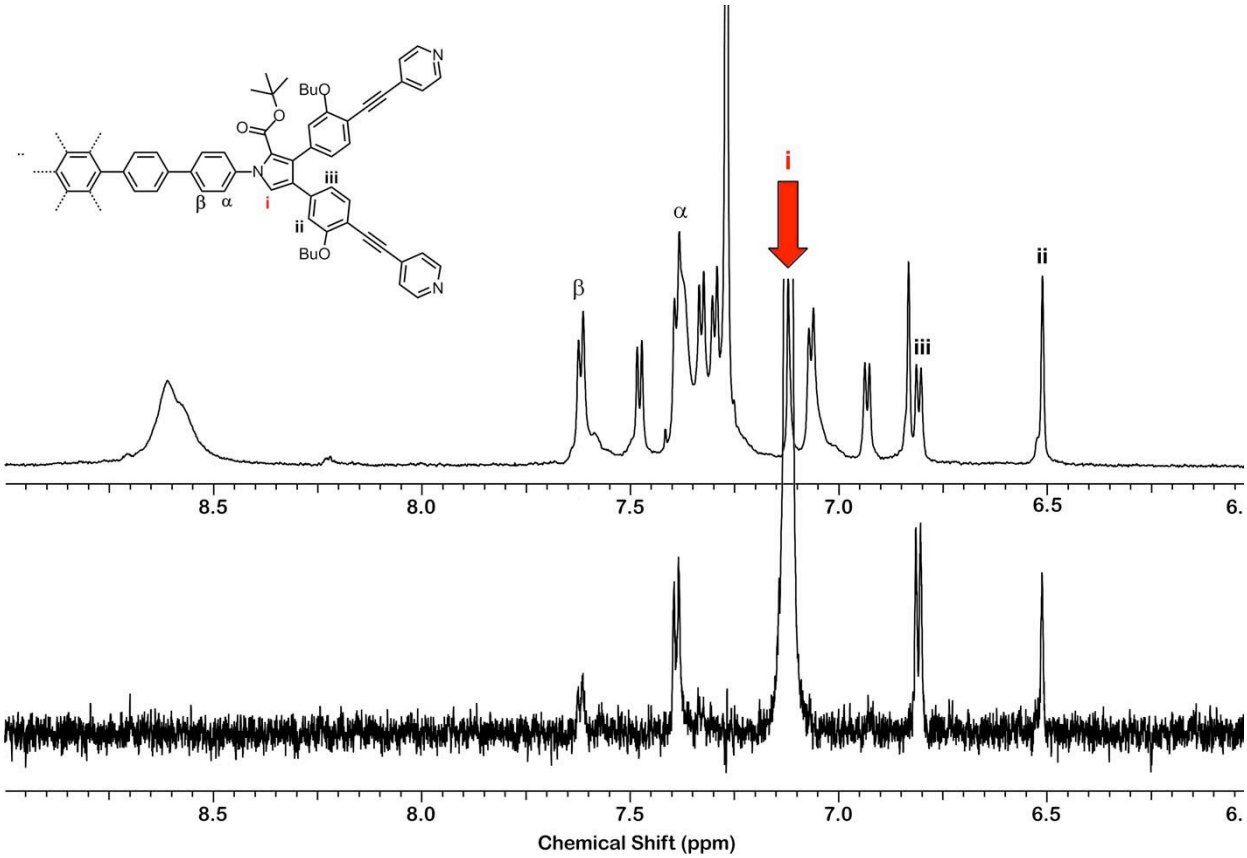

Figure S29. 1D NOE spectrum (700 MHz, $CDCl_3$, 298 K), irradiating the marked singlet at 7.12 ppm, corresponding to the pyrrolic proton i. A mixing time of 500 ms was used.

As expected, a 2D ROESY showed a strong NOE between protons γ and δ, but also allowed proton β to be assigned due to its proximity to γ (Figure S30). The α-δ assignments were confirmed by COSY correlations (Figure S31).

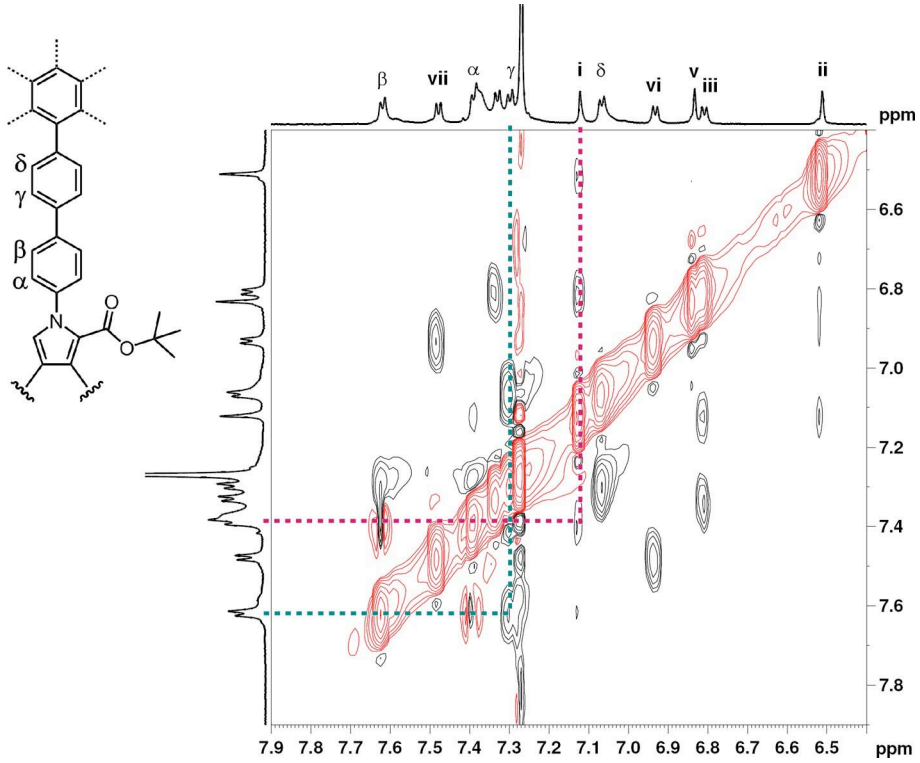

Figure S30. ^{1}H 2D ROESY spectrum (700 MHz, $CDCl_3$, 298 K) of 12-dentate template **T12**, showing crosspeaks between protons i-α, and β-γ. A mixing time of 200 ms was used (applied as a phase-alternating spin-lock pulse).

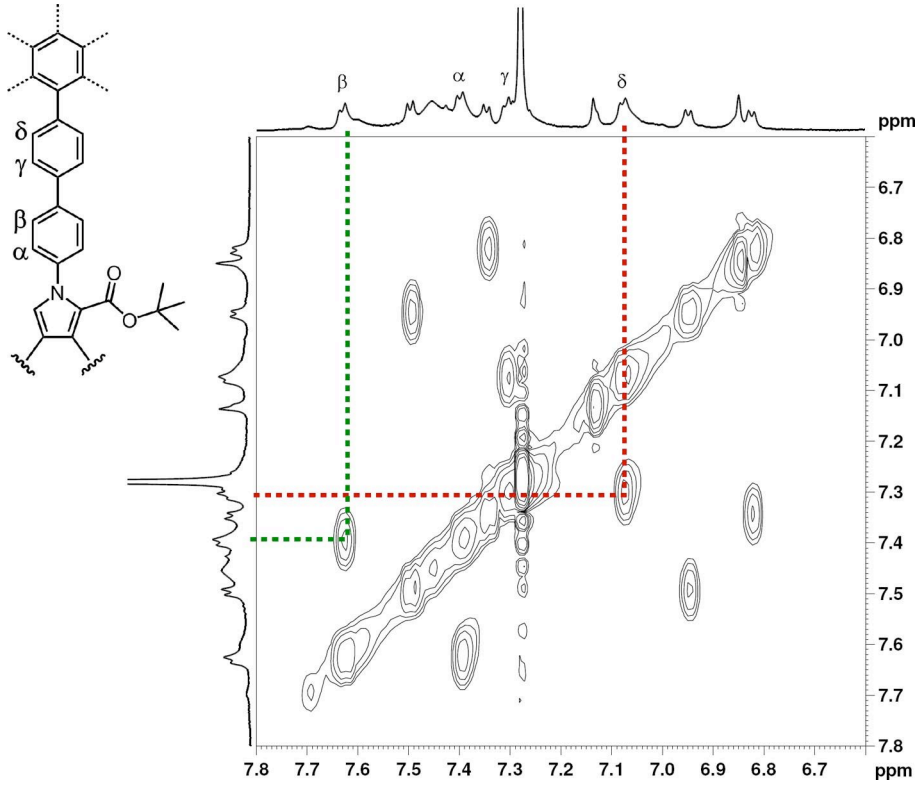

Figure S31. ^{1}H COSY spectrum (700 MHz, $CDCl_3$, 298 K) of 12-dentate template **T12**, showing crosspeaks between α-β and γ-δ.

B4b) MALDI mass spectrum

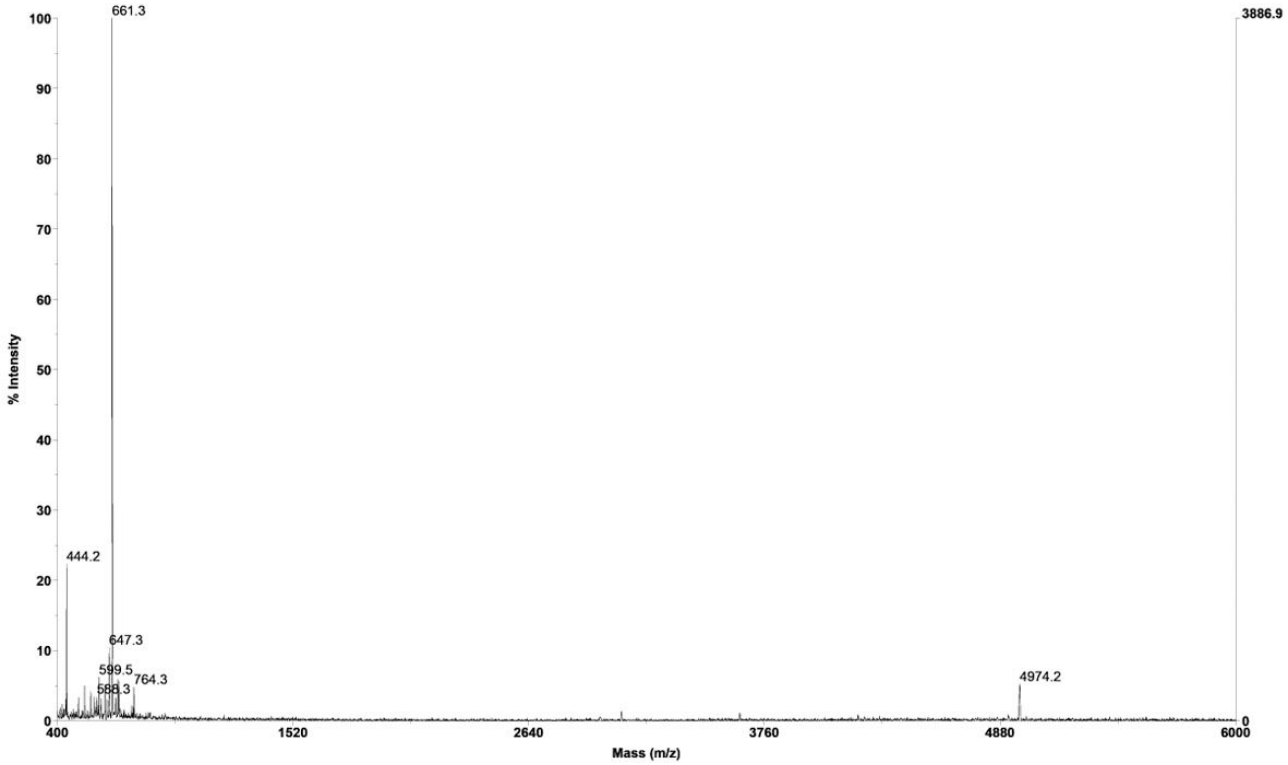

Figure S32. MALDI-ToF analysis of template **T12**. The peak at high molecular weight corresponds to the expected mass for **T12** (*m/z* 4974.2, expected 4974.1).

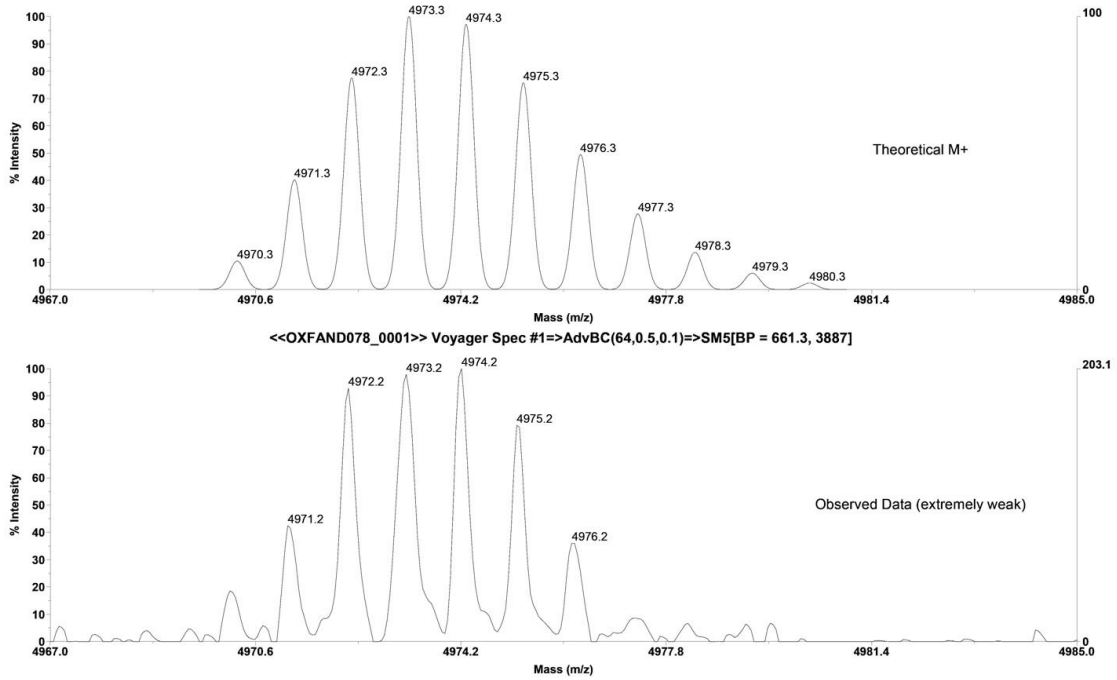

Figure S33. MALDI-ToF isotope patterning of template **T12** *(bottom)* and theoretical pattern calculated for $C_{336}H_{300}N_{18}O_{24}$ *(top)*.

*B5) Comparison of **c-P12** from both routes.*

Due to the complexity of the ^{1}H NMR spectrum of the [12]complex ***c*-P12·T12**, the template was removed, and the purity assessed using the resulting 12-porphyrin nanoring ***c*-P12** ^{1}H NMR and analytical GPC. Doping experiments, using the 12-porphyrin nanoring obtained by Vernier templating, were used to provide further proof of authenticity.

The 12-porphyrin nanoring ***c*-P12** obtained by templating the cyclisation of deprotected porphyrin tetramer with **T12** gave an identical retention time to that obtained by knockout of figure-of-eight ***c*-P12·(T6)$_2$** (Figure S34). The 12-porphyrin nanoring obtained by Vernier templating was co-injected with the crude cyclisation reaction mixture, and only one peak was observed.

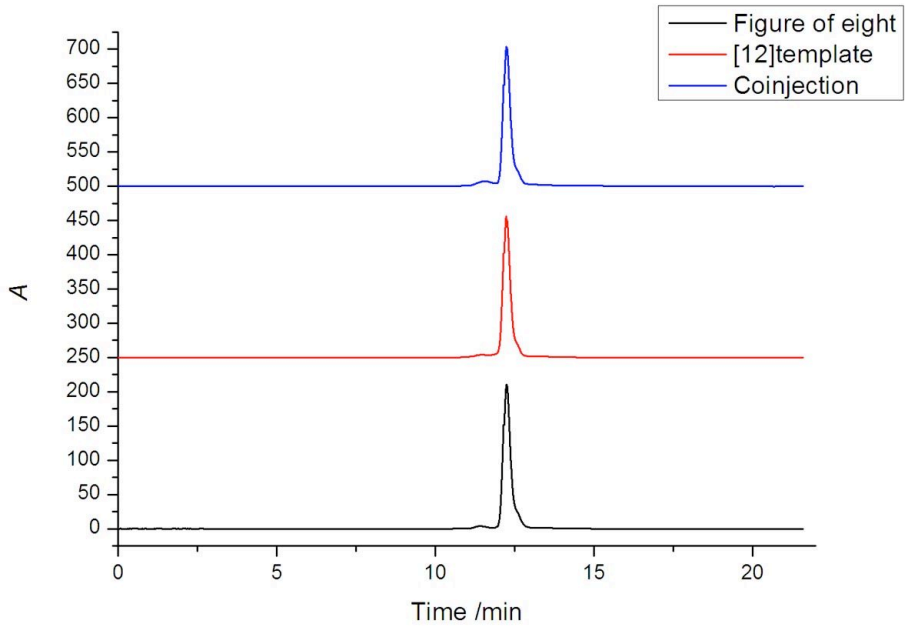

Figure S34. Analytical GPC (15% pyridine/toluene, 476 nm) traces of 12-porphyrin nanoring ***c*-P12** obtained by knockout of figure-of-eight *(black)*, and by 12-dentate template **T12** cyclisation *(red)*. Coinjection of both compounds *(blue)* shows perfect overlap of GPC peaks.

Similarly, the ^{1}H NMR spectra of 12-porphyrin nanoring ***c*-P12** from both routes were compared. Doping 12-porphyrin nanoring obtained by 12-dentate template cyclisation with that from the figure-of-eight knockout gave perfect overlap of the doublets arising from β-pyrrole protons (Figure S36). Difficulties in purification meant the ***c*-P12** sample obtained by 12-dentate template knockout was not as clean as that obtained by figure-of-eight knockout (Figure S35), further demonstrating the advantages of Vernier templating.

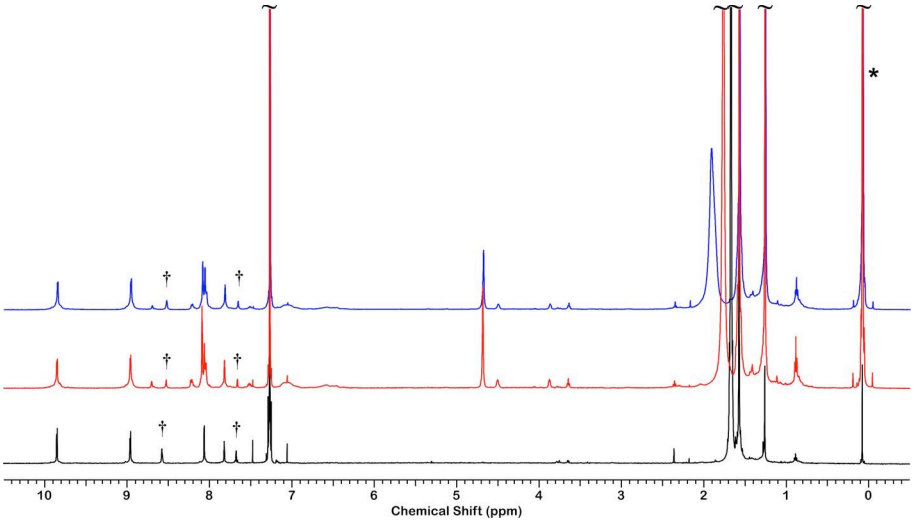

Figure S35. ^{1}H NMR spectra (500 MHz, $CDCl_3$/1% d_5-pyridine, 298 K) of 12-porphyrin nanoring ***c*-P12** obtained by figure-of-eight knockout *(black)*; by 12-dentate template cyclisation *(red)*; and a mixture of the two samples *(blue);* * indicates a silicon grease impurity; † indicates peaks due to pyridine.

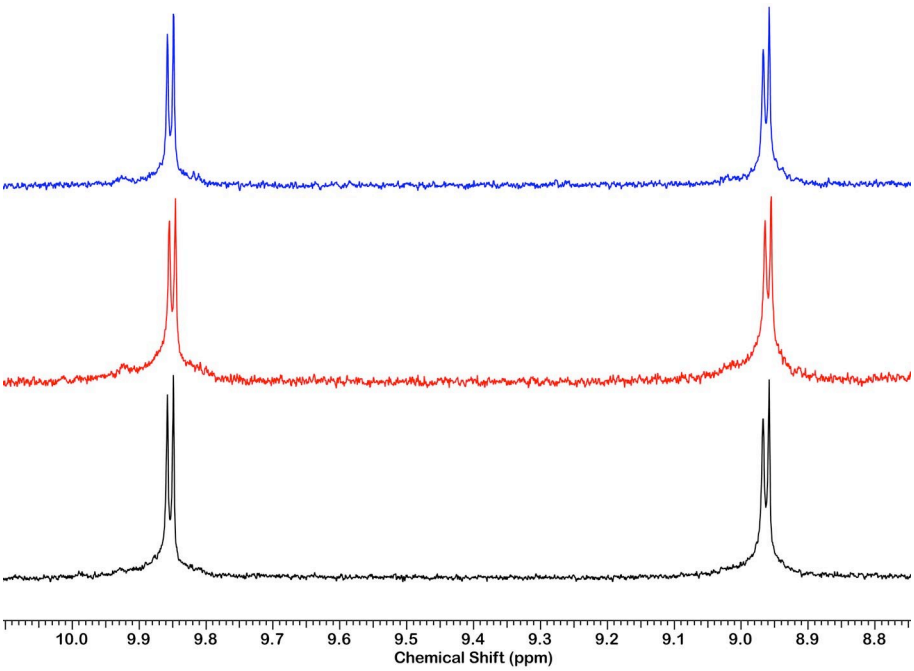

Figure S36. ^{1}H NMR spectra (500 MHz, $CDCl_3$/1% d_5-pyridine, 298 K) showing the porphyrin beta-pyrrole region of 12-porphyrin nanoring ***c*-P12** obtained by figure-of-eight knockout *(black)* and by 12-dentate template cyclisation *(red)*. Mixing both samples *(blue)* shows a perfect overlap of porphyrin peaks. [Expansion from Figure S35.]

The UV-vis spectra of 12-porphyrin nanoring from both sources also show a good match (Figure S37).

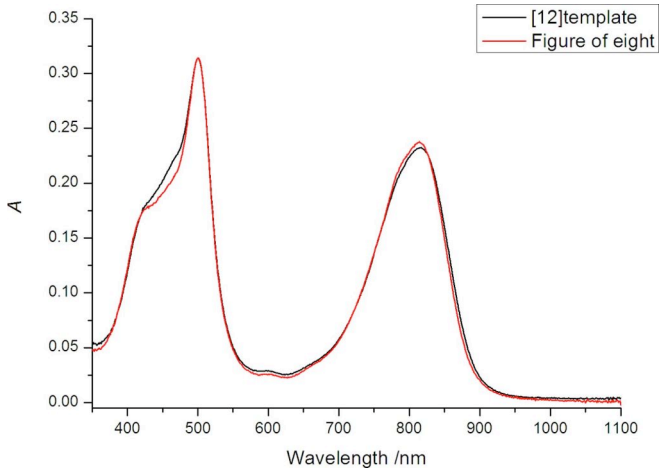

Figure S37. UV-vis absorption of 12-porphyrin nanoring ***c*-P12** obtained by cyclisation of deprotected tetramer bound to 12-dentate template **(*l*-P4)$_3$·T12** *(black)*, and that obtained by Vernier templating with hexadentate template **T6** *(red)*. Spectra in $CHCl_3$, [***c*-P12**] = 4.0×10^{-7} M^{-1}.

*B6) Molecular modelling of **c-P12·T12**.* Before synthesis, **T12** was modelled in HyperChem™ to ensure a good fit to the cavity of the free 12-porphyrin nanoring ***c*-P12** (Figure S38).

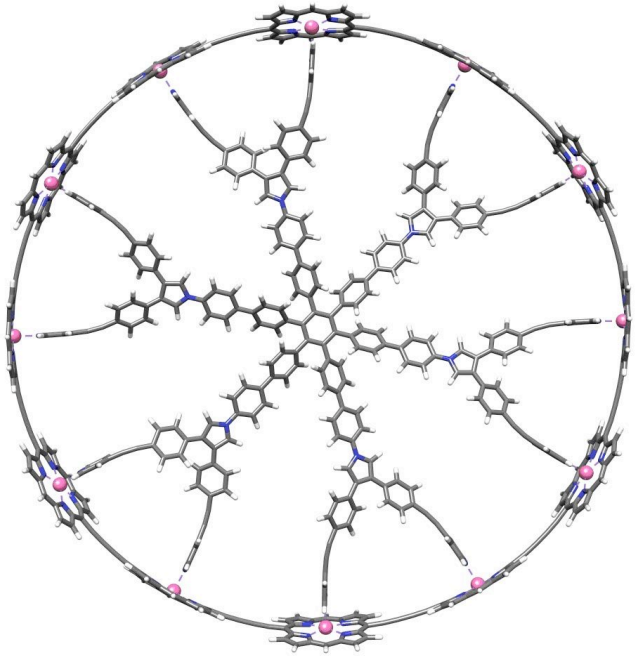

Figure S38. ***c*-P12·T12** modelled using the MM+ forcefield in HyperChem™ using an mm+ forcefield. Porphyrin *meso*-aryl, *n*-butyloxy and *t*-butyl ester groups are omitted from the model to simplify calculation.

The free cyclic porphyrin dodecamer ***c*-P12** has an optimised zinc-zinc distance (the distance between opposing zinc atoms) of 48.6 Å. A search of the Cambridge Structural Database (CSD) gives a mean zinc-nitrogen bond length of 2.2 Å,[S12] and an out of plane displacement (the distance the central zinc atom sits out of the porphyrin plane) of 0.3 Å, giving an ideal template nitrogen-nitrogen diameter (the distance between two opposing pyridyl arms) for the cavity of ***c*-P12** of 43.6 Å. Modelling **T12** in Hyperchem™ gave a mean nitrogen-nitrogen distance of 44.7 Å, only 1.1 Å larger than ideal.

C) Scanning tunnelling microscopy

C1) Preparation and Imaging of Gold Surface. A gold on mica substrate (4 mm × 8 mm, thickness 1500 Å; supplied commercially by Georg Albert-Physikal Vapour Deposition) was loaded into an ultra-high vacuum (UHV) system with a base pressure of 5×10^{-11} Torr. The sample was cleaned by Ar ion sputtering (5.5×10^{-6} Torr, 0.7 KeV, ~2.8 μA) and subsequent annealing (500° C). STM images were acquired using electrochemically etched tungsten tips, while operating in constant current mode at room temperature. Images of the surface obtained after the sputter anneal cycle show the characteristic (22 × √3) herringbone reconstruction of the Au(111) surface.[S13]

C2) Electrospray Deposition (ESD). ***c*-P12^{C8}** was dissolved in a toluene/methanol solution (3:1 by volume, with the addition of ~5% of pyridine to prevent aggregation) to give a concentration of ~200 μg/mL. During UHV-ESD, a bias of ~2 kV was applied to the emitter to produce the electrospray event. The presence of toluene and methanol within the preparation chamber, due to the introduction of the molecular beam, were detected by residual gas analysis.

Based on preliminary experiments with linear porphyrin oligomers and polymers bearing 3,5-(bisoctyloxy)phenyl sidegroups, we decided to use ***c*-P12^{C8}** rather than ***c*-P12** for STM studies. In the large area STM image, we see many nanometer-sized rings (Figure S38). Individual porphyrin units in the rings can be clearly identified and allow to determine the number of porphyrin units in each ring.

The sample of ***c*-P12^{C8}** used for the image in Figure 3c was prepared by Vernier templating from ***l*-P1** and **T6** whereas the sample used for the images in Figures S38 and S40 was synthesised from porphyrin monomer (***l*-P1**) as described in Section B6.

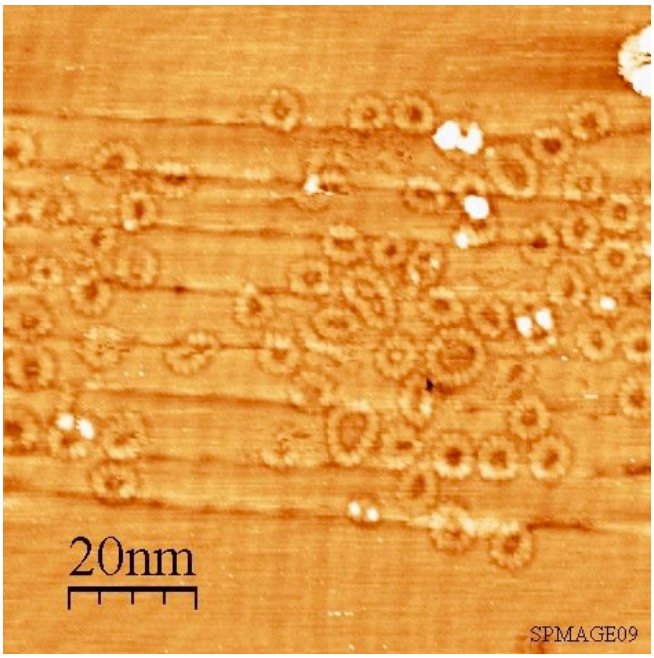

Figure S39. Large-area STM image of ***c*-P12^{C8}** on a Au(111) surface. The sample of ***c*-P12^{C8}** used for this experiment was synthesized from porphyrin monomer (***l*-P1**) as described in Section B6. As expected, most of the rings are cyclic dodecamer ***c*-P12^{C8}** (~90%), but a small number of larger rings comprising 18 porphyrin units (***c*-P18^{C8}**) can be identified as well (~5%). The presence of these rings can be explained with the formation of ***c*-P18·(T6)$_3$** during the synthesis.

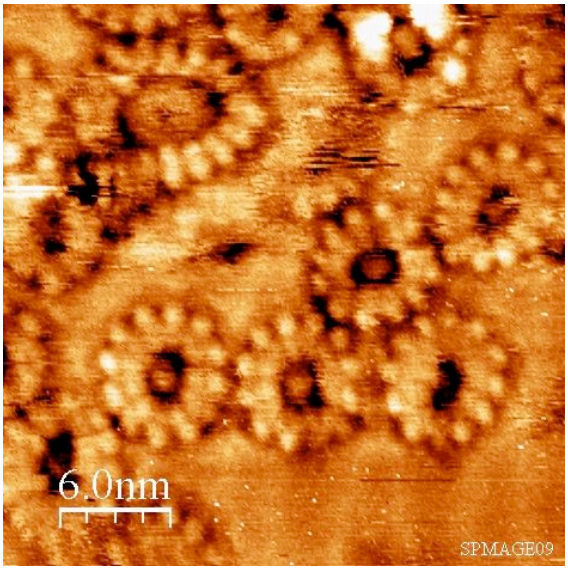

Figure S40. Small-area high-resolution STM image of ***c*-P12^{C8}** on a Au(111) surface. The sample of ***c*-P12^{C8}** used for this experiment was synthesised from porphyrin monomer (***l*-P1**) as described in Section B6.

D) References

S1 P. N. Taylor, H. L. Anderson, *J. Am. Chem. Soc.* **121**, 11538 (1999).
S2 M. Hoffmann, J. Kärnbratt, M.-H. Chang, L. M. Herz, B. Albinsson, H. L. Anderson, *Angew. Chem. Int. Ed.* **47**, 4993 (2008).
S3 X. Shen, D. M. Ho, R. A. Pascal, *J. Am. Chem. Soc.* **126**, 5798 (2004).
S4 F. Dötz, J. D. Brand, S. Ito, L. Gherghel, K. Müllen, *J. Am. Chem. Soc.* **122**, 7707 (2000).
S5 M. Hoffmann, C. J. Wilson, B. Odell, H. L. Anderson, *Angew. Chem. Int. Ed.* **46**, 3122 (2007).
S6 J. C. Antilla, J. M. Baskin, T. E. Barder, S. L. Buchwald, *J. Org. Chem.* **69**, 5578 (2004).
S7 D. I. Svergun, C. Berbato, M. H. J. Koch, *J. Appl. Cryst.* **28**, 768 (1995).
S8 E. Mylonas, D. I. Svergun, *J. Appl. Cryst.* **40**, s245 (2007).
S9 P. V. Konarev, V. V. Volkov, A. V. Sokolova, M. H. J. Koch, D. I. Svergun, *J. Appl. Cryst.* **36**, 1277 (2003).
S10 D. I. Svergun, *J. Appl. Cryst.* **25**, 495 (1992).
S11 K. L. Mardis, H. M. Sutton, X. Zuo, J. S. Lindsey, D. M. Tiede, *J. Phys. Chem. A.* **113**, 2516 (2009).
S12 R. M. Gomila, D. Quiñonero, A. Frontera, P. Ballester, P. M. Deyà, *J. Mol. Struc.: THEOCHEM* **531**, 381 (2000).
S13 J. V. Barth, H. Brune, G. Ertl, R. J. Behm, *Phys. Rev. B* **42**, 9307 (1990).